Age-related pacemaker deterioration is due to impaired intracellular and membrane mechanisms: Insights from numerical modeling

Joachim Behar and Yael Yaniv

Laboratory of Bioenergetic and Bioelectric Systems, Biomedical Engineering Faculty, Technion-Israel Institute of Technology, Haifa, Israel

Age-related deterioration of pacemaker function has been documented in mammals, including humans. In aged isolated sinoatrial node tissues and cells, reduction in the spontaneous action potential (AP) firing rate was associated with deterioration of intracellular and membrane mechanisms; however, their relative contribution to age-associated deficient pacemaker function is not known. Interestingly, pharmacological interventions that increase posttranslation modification signaling activities can restore the basal and maximal AP firing rate, but the identities of the protein targets responsible for AP firing rate restoration are not known. Here, we developed a numerical model that simulates the function of a single mouse pacemaker cell. In addition to describing membrane and intracellular mechanisms, the model includes descriptions of autonomic receptor activation pathways and posttranslation modification signaling cascades. The numerical model shows that age-related deterioration of pacemaker function is related to impaired intracellular and membrane mechanisms: HCN_4, T-type channels, and phospholamban functions, as well as the node connecting these mechanisms, i.e., intracellular Ca^{2+} and posttranslation modification signaling. To explain the restored maximal beating rate in response to maximal phosphodiesterase (PDE) inhibition, autonomic receptor stimulation, or infused cyclic adenosine monophosphate (cAMP), the model predicts that phospholamban phosphorylation by protein kinase A (PKA) and HCN_4 sensitivity to cAMP are altered in advanced age. Moreover, alteration in PKA and cAMP sensitivity can also explain age-reduced sensitivity to PDE inhibition and autonomic receptor stimulation. Finally, the numerical model suggests two pharmacological approaches and one gene manipulation method to restore the basal beating rate of aged pacemaker cells to that of normal adult cells. In conclusion, our numerical model shows that impaired membrane and intracellular mechanisms and the nodes that couple them can lead to deteriorated pacemaker function. By increasing posttranslation modification signaling, the deteriorated basal and maximal age-associated beating rate can be restored to adult levels.

The Journal of General Physiology

INTRODUCTION

The U.S. Administration on Aging estimates that by the year 2050, 20% of the population will be 65 y and older. By the year 2025, the number of individuals age 85 and older is projected to double and reach 8 million in the United States alone. At the same time, chronic cardiovascular diseases, e.g., coronary artery atherosclerosis, hypertension, and chronic heart failure, have reached epidemic proportions, and their incidence is growing exponentially, along with risks of disability with increasing age (Ogawa et al., 1992; Ferrari, 2002). Importantly, sinoatrial node (SAN) dysfunction increases exponentially with age, reaching an incidence of 1 of every 600 people ages 65 and older (Kusumoto and Goldschlager, 1996).

The SAN rate is controlled by both the autonomic nervous system (ANS) and intrinsic pacemaker mechanisms forming the coupled-clock system (Yaniv et al., 2015b). The ANS controls the beating rate by balancing the ratio of sympathetic to parasympathetic stimulation of G protein–coupled receptors: the sympathetic system stimulates β-adrenergic receptors (β-ARs), activating adenylyl cyclase (AC); the parasympathetic system stimulates cholinergic receptors, inactivating AC. In the cell, ATP is converted to cAMP by AC. The cAMP level controls PKA activity, and both cAMP and PKA determine the activation level of intrinsic pacemaker mechanisms: increased cAMP/PKA activity leads to an increase in the beating rate and vice versa (Yaniv et al., 2015a; Behar et al., 2016). In pacemaker cells, other types of AC exist (AC1 and AC8); these ACs are activated by intracellular Ca^{2+}, which is balanced by the interaction between membrane channels, exchangers, and pumps (membrane clock or M clock) and by internal Ca^{2+} storage (Ca^{2+} clock; Yaniv et al., 2013b). Both cAMP/PKA and intracellular Ca^{2+} serve as the node connecting the two clocks. Thus, deterioration in either clock's molecules or in ANS receptors can affect pacemaker function.

Correspondence to Yael Yaniv: yaely@bm.technion.ac.il

Abbreviations used: AC, adenylyl cyclase; ANS, autonomic nervous system; AP, action potential; β-AR, β-adrenergic receptor; CaMKII, Ca^{2+}/calmodulin-dependent protein kinase II; DD, diastolic depolarization; HCN channel, hyperpolarization-activated cyclic nucleotide–gated channel; HR, heart rate; IBMX, 3-isobutyl-1-methylxanthine; ISO, isoproterenol; LCR, local Ca^{2+} release; NCX, Na^+/Ca^{2+} exchanger; PDE, phosphodiesterase; PLB, phospholamban; SAN, sinoatrial node; SERCA, sarcoplasmic reticulum Ca^{2+} ATPase.

The Rockefeller University Press
J. Gen. Physiol. 2017
https://doi.org/10.1085/jgp.201711792

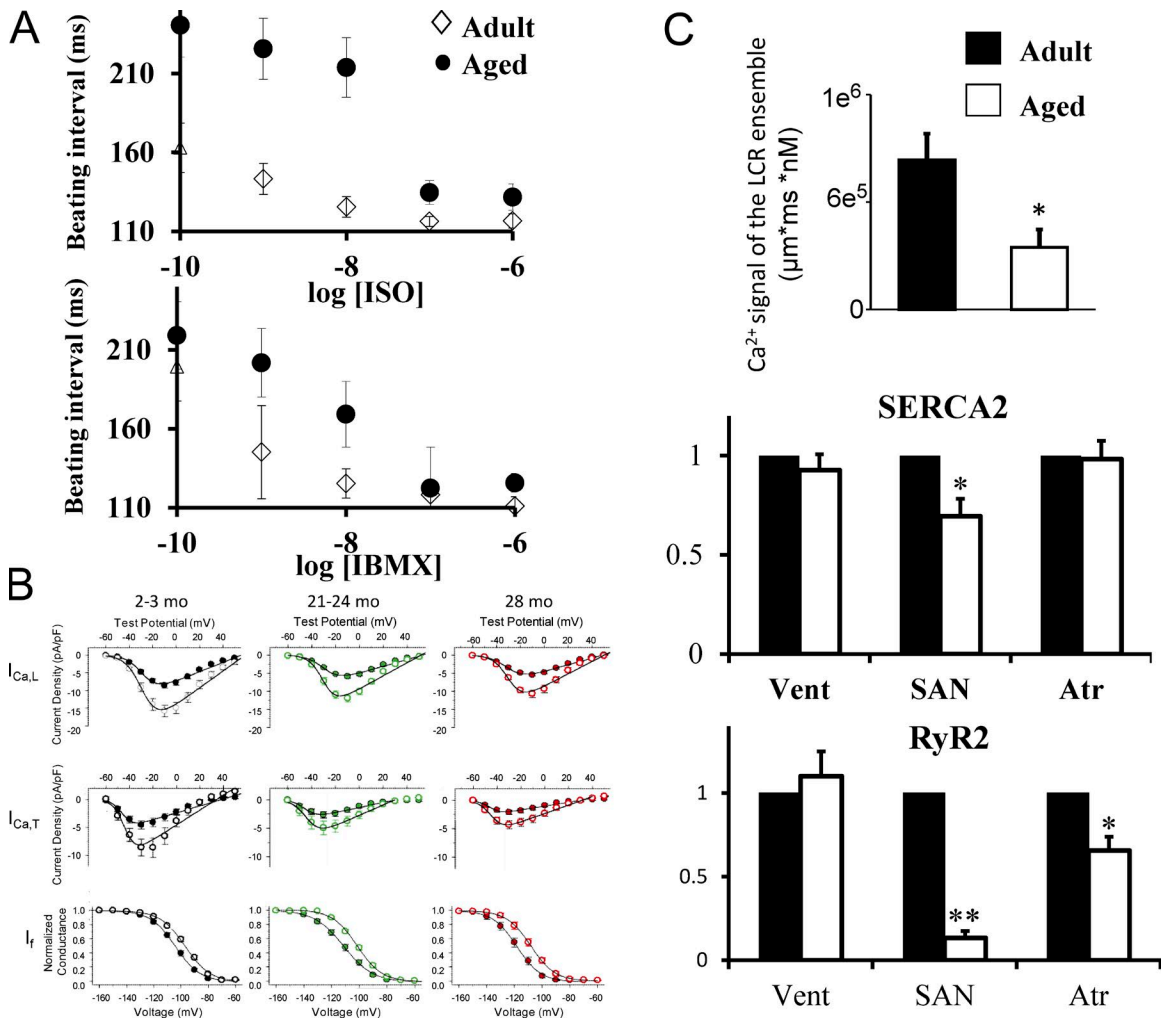

Figure 1. **Age-associated deficient pacemaker function.** (A) Age-associated reduction in basal beating interval and sensitivity to PDE inhibition by IBMX and β-AR stimulation by ISO. Note that the maximal beating rate is restored in response to maximal IBMX or ISO concentration (adapted from Yaniv et al. [2016]). Data are presented as mean ± SD. (B) Age-associated reduction in L-type, T-type, and HCN current conductance (adapted from Larson et al. [2013]) shown for sinoatrial node myocytes in mice aged 2–3 mo (black), 21–24 mo (green), and 28 mo (red) in the absence (filled circles) and presence (open circles) of 1 µM ISO. Data are presented as average ± SEM. (C) Age-associated reduced LCR ensemble, SERCA, and RyR2 presence (adapted from Liu et al. [2014]). From top to bottom: mean amplitudes of Ca^{2+} signals of the LCR ensemble (integrated Ca^{2+} signal produced by each LCR); representative Western blots of SAN (protein expression), atrial and ventricular tissues from adult (2–4 mo) and aged (24–27 mo) mice normalized to sarcomeric actin levels; RyR protein levels. Data are presented as mean ± SD. (top) *, $P < 0.05$ versus adult, mixed effects model for repeated measure ANOVA; (middle) *, $P < 0.05$ versus adult, two-tailed *t* test; (bottom) **, $P < 0.01$ versus adult; and *, $P < 0.05$, two-tailed *t* test.

Measurements of intrinsic (measured during autonomic blockade, precluding ANS effects) and maximal beating/heart rate (HR) provide evidence for deterioration in pacemaker function associated with aging. Although the basal HR (i.e., at rest) does not change in advanced age, the intrinsic HR declines with age in humans (Jose and Collison, 1970) and other mammals (Yaniv et al., 2016; Fig. 1 A). Because the intrinsic heart rate precludes ANS effects, its reduction reflects impaired activity of intrinsic pacemaker mechanisms: cAMP-PKA/Ca^{2+} signaling (Liu et al., 2014) and ionic channel currents (e.g., hyperpolarization-activated cyclic nucleotide–gated [HCN] channel and T-type and L-type Ca^{2+} channels; Larson et al., 2013; Fig. 1, B and C). However, the relative contribution of each mechanism to age-associated deterioration of pacemaker function is debatable. In contrast to the in vivo basal HR, the maximal HR declines in advanced age (Heath et al., 1981; Hagberg et al., 1985). Indeed recent data on pacemaker tissue (Liu et al., 2014; Yaniv et al., 2016) and data at the heart level (Brodde and Leineweber, 2004) have shown that the sensitivity to β-AR stimulation or phosphodiesterase (PDE) inhibition (using 3-isobutyl-1-methylxanthine [IBMX]) was reduced in advanced age. However, data have also shown that, in response to maximal autonomic receptor stimulation

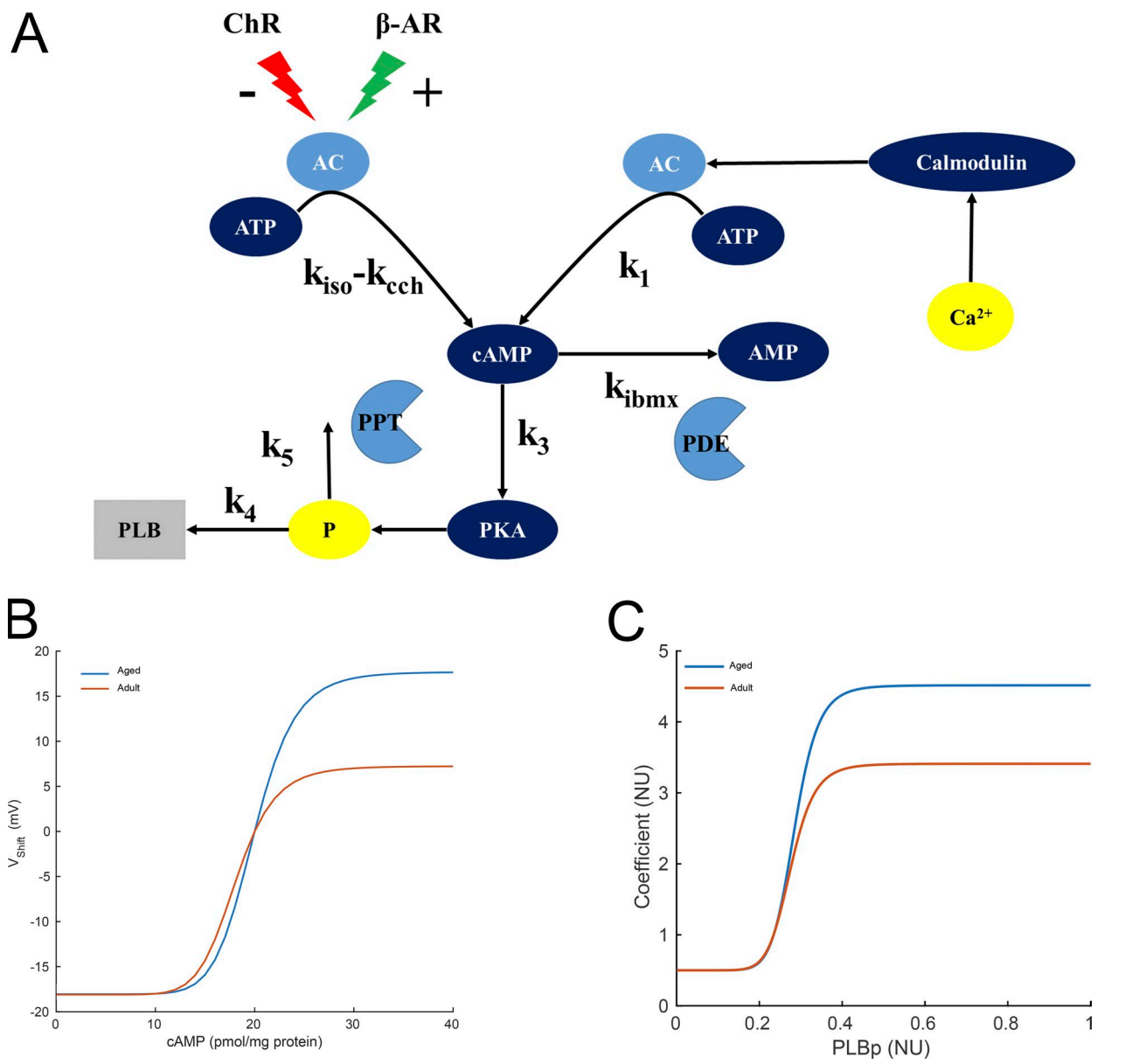

Figure 2. **Model parameters adjustment.** (A) Schematic illustration of the AC-AC-cAMP-PKA signaling cascade. AC is activated by adrenergic receptors (β-AR) and calmodulin and deactivated by cholinergic receptor (ChR) stimulation. Activated AC converts ATP into cAMP, which itself is transformed into PKA. PKA phosphorylates several targets, including PLB proteins, whose phosphorylation level will regulate the activation of SERCA and thus the rate at which Ca^{2+} enters the SR. The model includes two restraining mechanisms that act like brakes: protein phosphatase (PPT), which removes phosphate groups from proteins, and PDE, which breaks the phosphodiester bond in cAMP and degrades its level. (B) I_f shift in the I–V curve as a function of cAMP in adult and aged mice. Basal state (V shift = 0 and [cAMP] = 20 pmol/mg protein). The maximal shift for adult and aged mice was taken from the experimental results of Sharpe et al. (2017). (C) PLBp modulation of SERCA in adult and aged mice. The expressions for adult and aged mice are empirical.

or maximal increase in cAMP/PKA by PDE inhibition, the age-associated reduction in maximal beating rate can be compensated for. Nonetheless, the underlying biophysical mechanisms that allow this are not known. Numerical modeling is very useful, and sometimes it is the only feasible tool to explore such biophysical mechanisms. However, to date no aged pacemaker cell model exists.

Here, we used a numerical model of mouse pacemaker cells (Kharche et al., 2011) adapted to describe the effects of autonomic receptor stimulation. The model was used to answer three specific questions: (a) What is the relative contribution of each clock to the age-associated deterioration in pacemaker function? (b) What age-associated biophysical modulation makes it possible to compensate for the reduction in maximal

beating rate obtained in response to maximal PDE inhibition or β-AR stimulation? (c) Can the age-associated deterioration in pacemaker function be reversed by drug intervention or gene manipulation?

MATERIALS AND METHODS

Existing experimental results

Several groups have measured the reduction in the basal beating rate of either SAN tissue or single pacemaker cells from aged mice (Larson et al., 2013; Liu et al., 2014; Yaniv et al., 2016; Sharpe et al., 2017). Different mechanisms can cause the reduced pacemaker function: (a) reduced sarcoplasmic reticulum Ca^{2+} ATPase (SERCA) activity (Liu et al., 2014); (b) reduced RyR function (Liu et al., 2014); (c) shift of the half-activation potential of the HCN current (Sharpe et al., 2017); or (d) reduced L-type and T-type currents (Larson et al., 2013). Although the action potential (AP) sensitivity to β-AR (studied using isoproterenol [ISO]) or PDE inhibition (studied using IBMX) was reduced in advanced age (Yaniv et al., 2016), the maximal AP firing rate in response to these drugs (Yaniv et al., 2016) or to cAMP (Sharpe et al., 2017) was not significantly different between aged and young mice.

Basal numerical model

We adapted the Kharche et al. (2011) model for mouse pacemaker cells. This model was primarily based on experimental data from isolated mouse SAN cells. We updated the model based on Ca^{2+} measurements from Liu et al. (2014). For some ionic current parameters and biochemical signaling for which no mouse experimental data were available, we used the formulation from rabbit SAN cell models. The Kharche et al. (2011) model was updated to include the equations of cAMP-PKA signaling cascades and autonomic receptor stimulation (Yaniv et al., 2015a; Behar and Yaniv, 2016; Fig. 2 A). In addition, the following changes were made to the original model: the extracellular concentration of Ca^{2+} was changed to 2 mM according to Maltsev and Lakatta (2009); the intracellular concentration of Na^+ was changed from 8.1 to 10 mM as in the Maltsev–Lakatta model; the release rate parameter of the Ca^{2+} from the SR, k_s, was updated to 250,000 ms^{-1}, similar to the Maltsev–Lakatta model; the formulation of j_{up} to describe the Ca^{2+} pump rate was changed according to Kurata et al. (2002); and the conductance of I_{CaL} was increased by 18% and 38% for $g_{CaL1.2}$ and for $g_{CaL1.3}$, respectively. Finally, K^+ and Na^+ intracellular concentrations were kept constant, and I_{st} was removed from the model because it has no molecular basis (Maltsev et al., 2014). All model equations can be found in the supplement.

Model strategy

The effects of aging were simulated by varying the following model parameters: SERCA activity was decreased by 30%, as observed experimentally in Liu et al. (2014) (experimental data are presented in Fig. 1 C and are taken into account in Eqs. 20 and 22), and the conductance of I_{CaT} was decreased by 20% to simulate current density reduction during diastolic depolarization (DD), as found in Larson et al. (2013) (experimental data are presented in Fig. 1 B and are taken into account in Eqs. 23 and 24). In addition, Liu et al. (2014) showed changes in RyR function with a decrease in RyR activity in aged cells and a decrease in Ca^{2+} release of the local Ca^{2+} release (LCR) ensemble. To simulate these results, the release rate parameter of the Ca^{2+} from the SR, $k_s = 250{,}000\ ms^{-1}$, was decreased to $k_s = 87{,}500\ ms^{-1}$, i.e., decreased by a factor of 65%, corresponding to the experimental decrease in Ca^{2+} release of the LCR ensemble found in Liu et al. (2014) (Eqs. 29 and 30 and Fig. 1 C). The half-activation potential $V_{0.5}$ was changed in the HCN current equations from 104.2 mV in adult cells to 110 mV in aged cells (Sharpe et al., 2017; taken into account in Eqs. 14 and 17). The resulting decrease in the AP firing rate caused by aging was compared with published experimental data under basal conditions. In addition, the expression for the I–V curve of the HCN current was modified in the aged model (Fig. 2 B) to match the maximal shift found experimentally in the I–V curve under cAMP saturation (Sharpe et al., 2017), which was shown to be different from that of adults; ∼17 mV in aged cells versus ∼7 mV in adult cells (Sharpe et al., 2017). These values defined the maximal activation of $V_{0.5}$ by cAMP in adult and aged cells in our model (Fig. 2 B).

Cage release of cAMP was modeled as in our previous work (Behar and Yaniv, 2016). The effect of ISO was simulated using the equations developed in Yaniv et al. (2015a) and updated in Behar and Yaniv (2016) (Fig. 2 A). The effect of IBMX was simulated by decreasing the basal degradation rate of cAMP by PDE.

Model equations

cAMP activity

$$\frac{d[\mathrm{cAMP}]}{dt} = \left(k_{iso}\cdot[\mathrm{ATP}] + k_1\cdot[\mathrm{ATP}] - k_{ibmx}\cdot[\mathrm{cAMP}] - k_3\cdot[\mathrm{cAMP}] - k_{cch}\cdot[\mathrm{ATP}]\right)/60{,}000. \quad (1)$$

Our numerical model predicts that k_{iso} and k_{ibmx} are different for the adult and aged cases (see Results for further details).

Adult

$$k_{iso,adult} = 0.1599\cdot\frac{[\mathrm{ISO}]^{0.6238}}{76.5441^{0.6238} + [\mathrm{ISO}]^{0.6238}}, \quad (2)$$

$$k_{ibmx,\ adult} = -0.8730 \cdot \frac{[\mathrm{IBMX}]^{0.8395}}{4.0550^{0.8781} + [\mathrm{IBMX}]^{0.8395}} + 1. \quad (3)$$

Aged

$$k_{iso,aged} = 0.1434 \cdot \frac{[\mathrm{ISO}]^{2.0704}}{334.2799^{2.0704} + [\mathrm{ISO}]^{2.0704}}, \quad (4)$$

$$k_{ibmx,\ aged} = -0.9118 \cdot \frac{[\mathrm{IBMX}]^{0.8781}}{47.6705^{0.8781} + [\mathrm{IBMX}]^{0.8781}} + 1, \quad (5)$$

$$k_{cch} = 0.0146 \cdot \frac{[\mathrm{CCh}]^{1.4402}}{51.7331^{1.4402} + [\mathrm{CCh}]^{1.4402}}, \quad (6)$$

$$k_1 = K_{AC,I} + \frac{K_{AC}}{1 + \exp\left(\left(K_{Ca} - k_{bCM} \cdot \frac{f_{CMi}}{k_{fCM} \cdot (1 - f_{CMi})}\right) / K_{AC,Ca}\right)}, \quad (7)$$

$$k_2 = k_{ibmx} \cdot 265.3512 \cdot \frac{[\mathrm{cAMP}]^{5.7343}}{24.7290^{6.7343} + [\mathrm{cAMP}]^{6.7343}}, \quad (8)$$

$$k_3 = k_{PKA} \cdot \frac{[\mathrm{cAMP}]^{(n_{PKA}-1)}}{k_{PKA,cAMP}^{n_{PKA}} + [\mathrm{cAMP}]^{n_{PKA}}}. \quad (9)$$

In addition, in the aged-model equations that follow, two additional changes were made to the cAMP activation curve for I_f and the phospholamban (PLB) sensitivity to PKA phosphorylation (see Results and Fig. 2 C for further details).

Hyperpolarization activated "funny" current, I_f

$$I_{fNa} = 0.3833 \cdot g_{If} \cdot (V_m - E_{Na}) \cdot y, \quad (10)$$

$$I_{fK} = 0.6167 \cdot g_{If} \cdot (V_m - E_K) \cdot y. \quad (11)$$

Adult

$$K_{if} = 25.3403,\ K_{0.5if} = 18.1115,\ n_{if} = 9.6383, \quad (12)$$

$$V_{shift} = K_{if} \cdot \frac{[\mathrm{cAMP}]^{n_{if}}}{K_{0.5if}^{n_{if}} + [\mathrm{cAMP}]^{n_{if}}} - 18.1040, \quad (13)$$

$$y_\infty = \frac{1}{1 + \exp((V_m + 104.2 - V_{shift})/16.3)}. \quad (14)$$

Aged

$$K_{if} = 35.7355,\ K_{0.5if} = 19.9587,\ n_{if} = 9.6383, \quad (15)$$

$$V_{shift} = K_{if} \cdot \frac{[\mathrm{cAMP}]^{n_{if}}}{K_{0.5if}^{n_{if}} + [\mathrm{cAMP}]^{n_{if}}} - 18.0457, \quad (16)$$

$$y_\infty = \frac{1}{1 + \exp((V_m + 110 - V_{shift})/16.3)}, \quad (17)$$

$$\tau_y = 1.5049 / \begin{pmatrix} \exp(-(V_m + 590.3) \cdot 0.01094) + \\ \exp((V_m - 85.1)/17.2) \end{pmatrix}. \quad (18)$$

The rate of Ca^{2+} uptake (pumping) by the SR, j_{up}

Adult

$$f([\mathrm{PLB_p}]) = 2.9102 \cdot \frac{[\mathrm{PLB_p}]^{9.5517}}{0.2763^{9.5517} + [\mathrm{PLB_p}]^{9.5517}} + 0.4998, \quad (19)$$

$$j_{up} = P_{up,basal} \cdot \frac{f([\mathrm{PLB_p}])}{1 + K_{up}/[\mathrm{Ca^{2+}}]_i}. \quad (20)$$

Aged

$$f([\mathrm{PLB_p}]) = 4.0152 \cdot \frac{[\mathrm{PLB_p}]^{9.9463}}{0.2853^{9.9463} + [\mathrm{PLB_p}]^{9.9463}} + 0.4999, \quad (21)$$

$$j_{up} = 0.7 * P_{up,basal} \cdot \frac{f([\mathrm{PLB_p}])}{1 + K_{up}/[\mathrm{Ca^{2+}}]_i}. \quad (22)$$

T-type Ca^{2+} current, I_{CaT}

Adult

$$I_{CaT} = g_{CaT} \cdot (V_m - E_{CaT}) \cdot d_T \cdot f_T. \quad (23)$$

Aged

$$I_{CaT} = 0.8 \cdot g_{CaT} \cdot (V_m - E_{CaT}) \cdot d_T \cdot f_T, \quad (24)$$

$$d_{T\infty} = \frac{1}{1 + \exp(-(V_m + 26)/6)}, \quad (25)$$

$$f_{T\infty} = \frac{1}{1 + \exp((V_m + 61.7)/5.6)}, \quad (26)$$

$$\tau_{dT} = 1 / \begin{pmatrix} 1.068 \cdot \exp((V_m + 26.3)/30) + \\ 1.068 \cdot \exp(-(V_m + 26.3)/30) \end{pmatrix}, \quad (27)$$

$$\tau_{fT} = 1 / \begin{pmatrix} 0.0153 \cdot \exp(-(V_m + 61.7)/83.3) + \\ 0.015 \cdot \exp((V_m + 61.7)/15.38) \end{pmatrix}. \quad (28)$$

RyR function

Adult

$$j_{SRCarel} = k_s \cdot OO \cdot ([\mathrm{Ca^{2+}}]_{\mathrm{jSR}} - [\mathrm{Ca^{2+}}]_{\mathrm{sub}}). \quad (29)$$

Aged

$$j_{SRCarel} = 0.35 \cdot k_s \cdot OO \cdot ([\mathrm{Ca^{2+}}]_{\mathrm{jSR}} - [\mathrm{Ca^{2+}}]_{\mathrm{sub}}), \quad (30)$$

$$k_{CaSR} = MaxSR - \frac{MaxSR - MinSR}{1 + (EC_{50SR}/[\mathrm{Ca^{2+}}]_{\mathrm{jSR}})^{HSR}},$$

$$k_{oSRCa} = k_{oCa}/k_{CaSR},$$

$$k_{iSRCa} = k_{iCa} \cdot k_{CaSR},$$

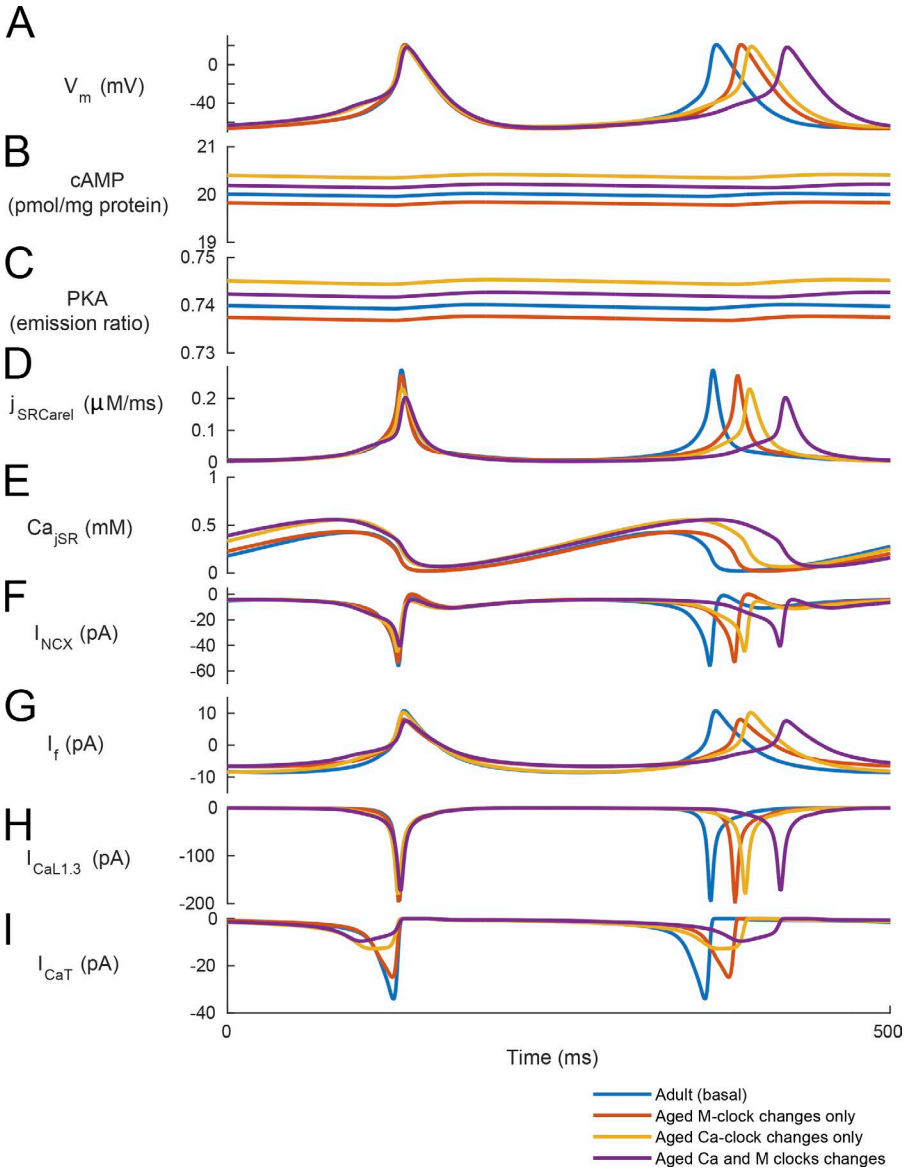

Figure 3. **Model simulation in response to changes occurring with aging.** Coupled-clock function of adult mice (blue), aged mice when only changes in the M clock mechanisms were taken into account (red), aged mice when only changes in the Ca^{2+} clock mechanisms were taken into account (yellow), and aged mice when changes in both M and Ca^{2+} clock mechanisms were included (purple). Membrane voltage, main membrane currents, AC-cAMP-PKA signaling, and Ca^{2+} cycling (flux and concentration) in the SR in adult and aged mice: membrane voltage (V_m; A); cAMP level (B); PKA activity level (C); flux of Ca^{2+} existing in the SR ($j_{SRCarel}$; D); Ca^{2+} concentration in the junctional SR compartment (Ca_{jSR}; E); the Na^{+}-Ca^{2+} exchanger current (I_{NCX}; F); HCN current (I_f; G; L-type current (I_{CaL}; H); and T-type Ca^{2+} current (I_{CaT}; I).

$$dR/dt = \left(k_{im} \cdot RI - k_{iSRCa} \cdot \left[Ca^{2+}\right]_{sub} \cdot R\right) - \left(k_{oSRCa} \cdot \left[Ca^{2+}\right]_{sub}^{2} \cdot R - k_{om} \cdot OO\right),$$

$$dOO/dt = \left(k_{oSRCa} \cdot \left[Ca^{2+}\right]_{sub}^{2} \cdot R - k_{om} \cdot OO\right) - \left(k_{iSRCa} \cdot \left[Ca^{2+}\right]_{sub} \cdot OO - k_{im} \cdot S\right),$$

$$dS/dt = \left(k_{iSRCa} \cdot \left[Ca^{2+}\right]_{sub} \cdot OO - k_{im} \cdot S\right) - \left(k_{om} \cdot S - k_{oSRCa} \cdot \left[Ca^{2+}\right]_{sub}^{2} \cdot RI\right),$$

$$dRI/dt = \left(k_{om} \cdot S - k_{oSRCa} \cdot \left[Ca^{2+}\right]_{sub}^{2} \cdot RI\right) - \left(k_{im} \cdot RI - k_{iSRCa} \cdot \left[Ca^{2+}\right]_{sub} \cdot R\right).$$

The software was developed in Matlab (MathWorks). Numerical integration was performed using the Matlab ode15s stiff solver, and the model simulations were run for 2,000 s to ensure that steady state was reached. Computation was performed on an Intel Core i7-4790 CPU at 3.60 GHz with 8 GB of RAM.

All model equations and parameters (Tables S1 and S2) appear in the supplement. The source code of the numerical model is available at http://bioelectric-bioenergetic-lab.net.technion.ac.il.

Online supplemental material

Table S1 shows coupled differential equation variables in the initial conditions. Table S2 shows model constants. The supplemental text shows all model equations.

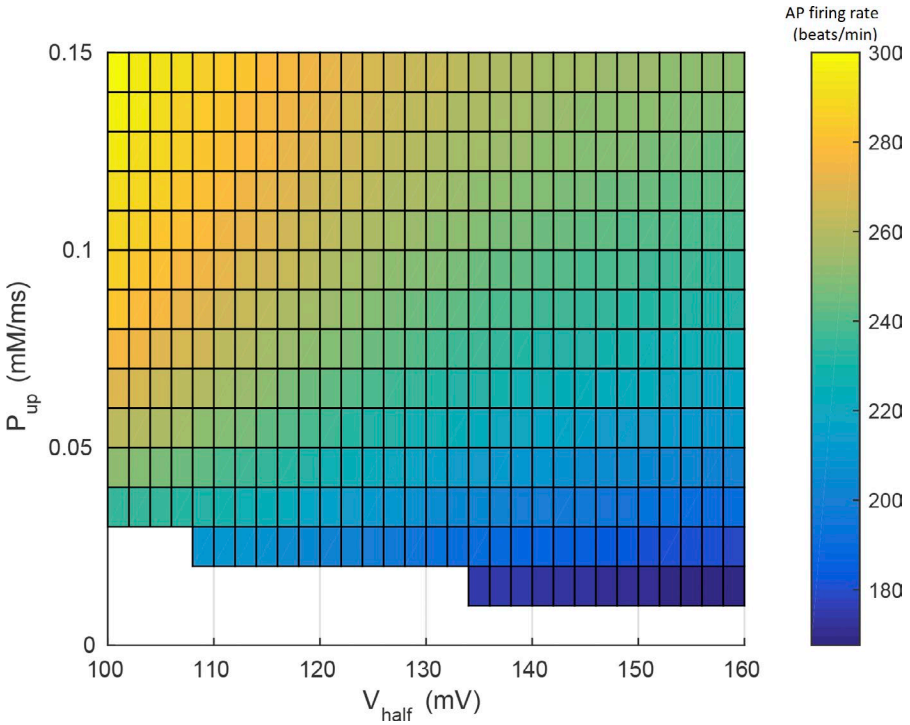

Figure 4. **Parameter sensitivity to *Pup* and $V_{0.5}$.** The effect of changes in P_{up} and $V_{0.5}$ on AP firing rate. $V_{0.5}$ refers to the half activation voltage of the HCN current, I_f.

RESULTS

Mechanisms associated with both the M and Ca^{2+} clock contribute to the age-deteriorated pacemaker function

To explore the relative role of M and Ca^{2+} clock components in age-associated deterioration of pacemaker function, we used our numerical model. Fig. 3 shows the coupled-clock function of adult mice, aged mice when only changes in the M clock mechanisms were taken into account (Fig. 1 B), aged mice when only changes in the Ca^{2+} clock mechanisms were taken into account (Fig. 1 C), and aged mice when changes in both M and Ca^{2+} clock mechanisms were included. The numerical model simulations show that only when mechanisms associated with both the M and Ca^{2+} clocks are taken into account does the reduction in spontaneous AP firing rate match the experimental results (Larson et al., 2013). Fig. 3 shows that age-reduced pacemaker function was associated with reduced release of Ca^{2+} from the RyR (reduced $j_{SRCarel}$), small elevation in SR load (less release compared with sequestration of Ca^{2+}), and reduction in I_f, I_{NCX}, $I_{Ca,L}$, and $I_{Ca,T}$. Quantitatively, the peak amplitude of $j_{SRCarel}$ changed from 0.291 µM/ms in adult cells to 0.20 µM/ms in aged cells, and the amount of Ca^{2+} ejected over one cycle was 8.14 µM in adult cells and 7.69 µM in aged cells.

Although we changed SERCA activity, HCN current conductivity, and RyR kinetics in accordance with experimental data (Fig. 1), we also performed parameter sensitivity analysis to prove that the model predictions are not dependent on only one set of parameters. Fig. 4 shows the changes in AP firing rate in the aged model in response to changes in $V_{1/2}$ of the HCN channel or in response to changes in P_{up} of the SERCA. Moreover, the range we chose for P_{up} allowed us not only to reproduce the experimental results, but also to provide a stable beating rate (Fig. 4).

Reduction in I_{NCX}, I_{Na}, I_K, or I_{NaK} can deteriorate age-dependent pacemaker function

Although age-dependent changes of RyR, SERCA, PLB, $I_{Ca,L}$, $I_{Ca,T}$, and I_f have been reported, no data exist on changes of I_{NCX}, I_{Na}, I_K, or I_{NaK}. However, the numerical model can illustrate the indirect result of other pacemaker functions caused by the coupled-clock effect. Fig. 5 illustrates all currents for the basal adult and aged cases. I_{NCX} amplitude decreases significantly with aging (Fig. 5 J), I_{Kr} and I_{NaK} density (Fig. 5, D and K) are higher during early DD in aged cells, and the density of I_{Na} (Fig. 5, G and H) is lower during DD, but with a peak amplitude more shifted to the early DD. The net effect of all coupled-clock changes is a slower AP upstroke during DD in aged cells than in adult cells, thus leading to a lower AP firing rate.

Age-associated modification in I_f sensitivity to cAMP and PLB sensitivity to PKA can explain the restoration of age-deteriorated pacemaker function

We next simulated the changes in spontaneous AP firing rate in response to maximal ISO, IBMX, or cAMP concentration. Fig. 6 shows that in response to any of these drugs (which bring the beating rate to its maximal value), the spontaneous AP firing rate in aged pacemaker cells is lower than in adult cells. However, these results contra-

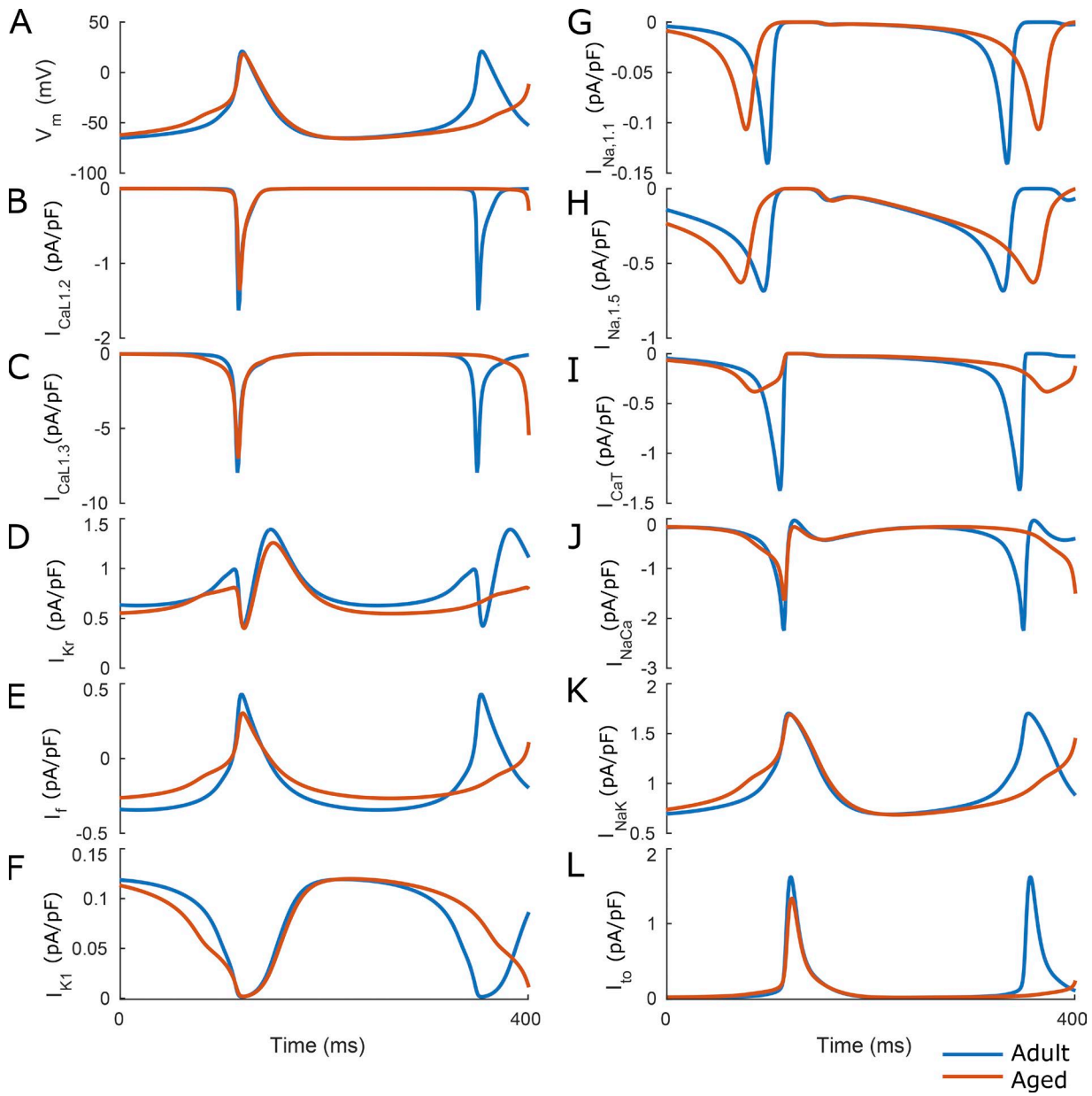

Figure 5. **Major currents in adult and aged mice.** Modification in specific membrane and sarcoplasmic proteins (I_{CaT}, RyR, I_f) modified the other proteins. (A) Membrane voltage (V_m). (B) 1.2 L-type current ($I_{CaL1.2}$). (C) 1.3 L-type current ($I_{CaL1.2}$). (D) Rapidly activating delayed rectifier K^+ current (I_{Kr}). (E) HCN current. (F) Inward rectifying K^+ current (I_{K1}). (G) Sodium current ($I_{Na1.1}$). (H) Sodium current ($I_{Na1.5}$). (I) T-type Ca^{2+} current (I_{CaT}). (J) Na^+-Ca^{2+} exchanger current (I_{NaCa}). (K) Na^+-K^+ pump current (I_{NaK}). (L) 4-aminopyridine–sensitive currents (I_{to}).

dict recently published data (Liu et al., 2014; Yaniv et al., 2016). The model was modified to fit the experimental data: we searched for modifications in clock mechanisms that could bring the maximal spontaneous AP firing rate of aged cells to the one simulated for adults. We focused on two targets, age-dependent modification in HCN4 sensitivity to cAMP and PLB sensitivity to PKA. Fig. 6 shows that modification of HCN4 sensitivity to cAMP in aged cells can partially restore the maximal age-deteriorated pacemaker AP firing rate to the adult level, but not to the level documented experimentally. We modified PLB sensitivity to PKA so that the maximal heart rate in response to ISO or IBMX stimulation will fit the experimentally published levels (Liu et al., 2014; Yaniv et al., 2016). Only when the modification in PLB sensitivity to PKA (see Materials and methods, Eqs. 19, 20, 21, and 22) was also taken into account could the maximal AP firing rate of aged pacemaker cells be restored to the adult level. Note that although there is a slight difference between the final predicted maximal heart rate of adult and aged pacemaker cells, this difference is not significant and cannot not be measured experimentally.

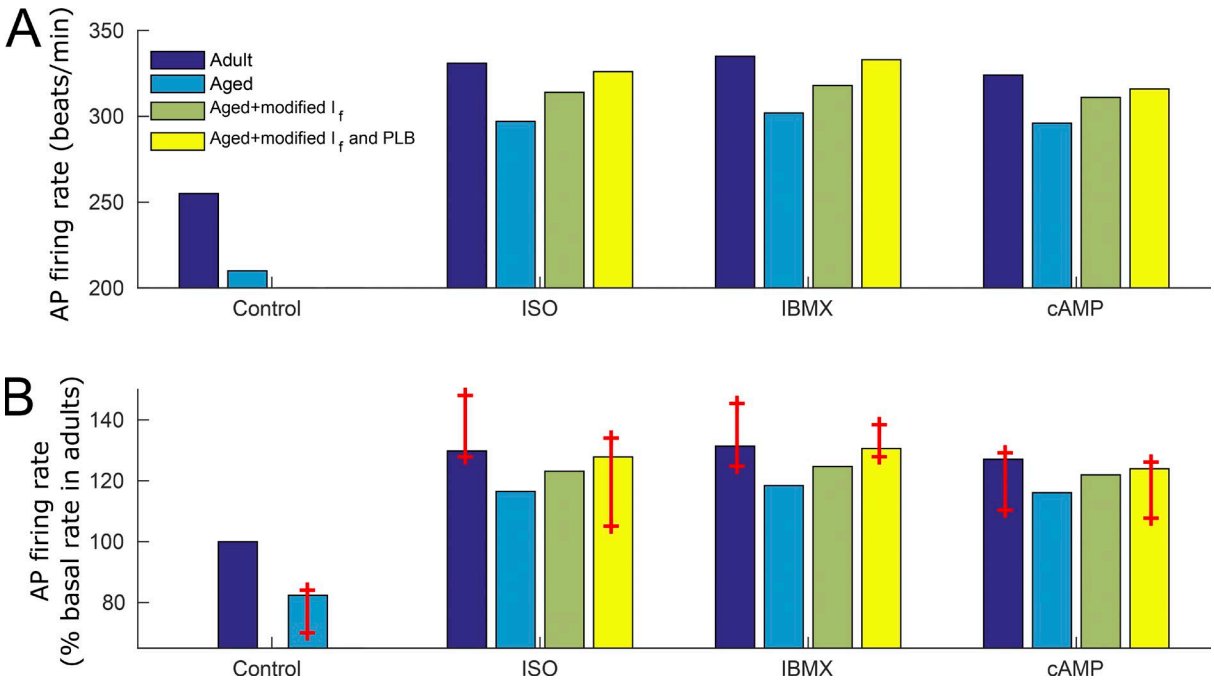

Figure 6. **Mean AP firing rate changes in response to drug perturbations.** Simulated AP firing rate in absolute numbers (A) and percentage change from the adult basal firing rate (B) of young and adult mouse SAN cells under ISO (1,000 µM), caged cAMP release, or IBMX treatment (3,000 µM). In B, the red bars show the experimental range (defined as mean ± twice the SEM) of the decrease in AP firing rate in aged cells with respect to the adult basal rate, as reported in Larson et al. (2013), Liu et al. (2014), and Sharpe et al. (2017).

Figs. 7 and 8 show how the coupled-clock mechanisms lead to restored maximal pacemaker function. In response to maximal concentration of ISO (Fig. 7), cAMP and PKA are restored, the release of Ca^{2+} is compensated for, more Ca^{2+} is accumulated in the SR because the rate of Ca^{2+} sequestration is higher than the rate of release, and I_f, I_{NCX}, $I_{Ca,L}$, and $I_{Ca,T}$ are all completely or partly restored. In response to maximal concentration of IBMX (Fig. 8), similar changes in coupled-clock mechanisms occur.

Age-associated modification in I_f sensitivity to cAMP and PLB sensitivity to PKA can explain the reduced sensitivity of pacemaker function to external and internal stimuli

Experimental data show that the sensitivity to either PDE inhibition (by IBMX) or β-AR receptor stimulation (by ISO) is reduced in advanced age (Yaniv et al., 2016). Our numerical model could reproduce these results only when $k_{iso,aged}$ and $k_{ibmx,aged}$ (Eqs. 4 and 5) were modified with respect to their adult expression. Thus, the model predicts that in aged cells, the response to ISO or IBMX stimulation is different than in adult pacemaker cells. This age-related modification was generated to match the drug dose–dependent results that were reported experimentally (Yaniv et al., 2016). Fig. 9 shows that higher concentrations of ISO or IBMX are needed to achieve the same percentage of increase in spontaneous AP firing rate. Based on the numerical model results, the age-associated EC_{50} was ∼203 nM for ISO and 26 µM for IBMX compared with ∼11 nM and ∼6.3 µM in adults in response to ISO and IBMX, respectively. Note that these results can be obtained only by age-associated modification in HCN_4 sensitivity to cAMP and PLB sensitivity to PKA.

The age-associated basal AP firing rate can be reversed

The numerical model was used to predict whether the age-associated decrease in basal beating rate can be reversed using drug perturbations or gene manipulation. Fig. 10 A shows that 167 nM ISO can reverse the aged basal AP firing rate to that of adult mouse pacemaker cells. Fig. 10 B shows that 50 µM IBMX can also reverse the aged basal AP firing rate to that of adult mouse pacemaker cells. Thus, using pharmacological interventions, the old heart can be made adult again. A recent patent (Maltsev et al., 2016) suggests that overexpression of AC1 or AC8 can lead to restoration of normal beating rate. Fig. 11 shows that increasing the presence of AC1 and AC8 (by increasing K_{AC}) reverses the age-associated decrease in beating rate and restores it to the adult level.

DISCUSSION

Our first major conclusion is that both the M and Ca^{2+} clocks contribute to the deterioration of basal pacemaker function in advanced age (Fig. 3). This con-

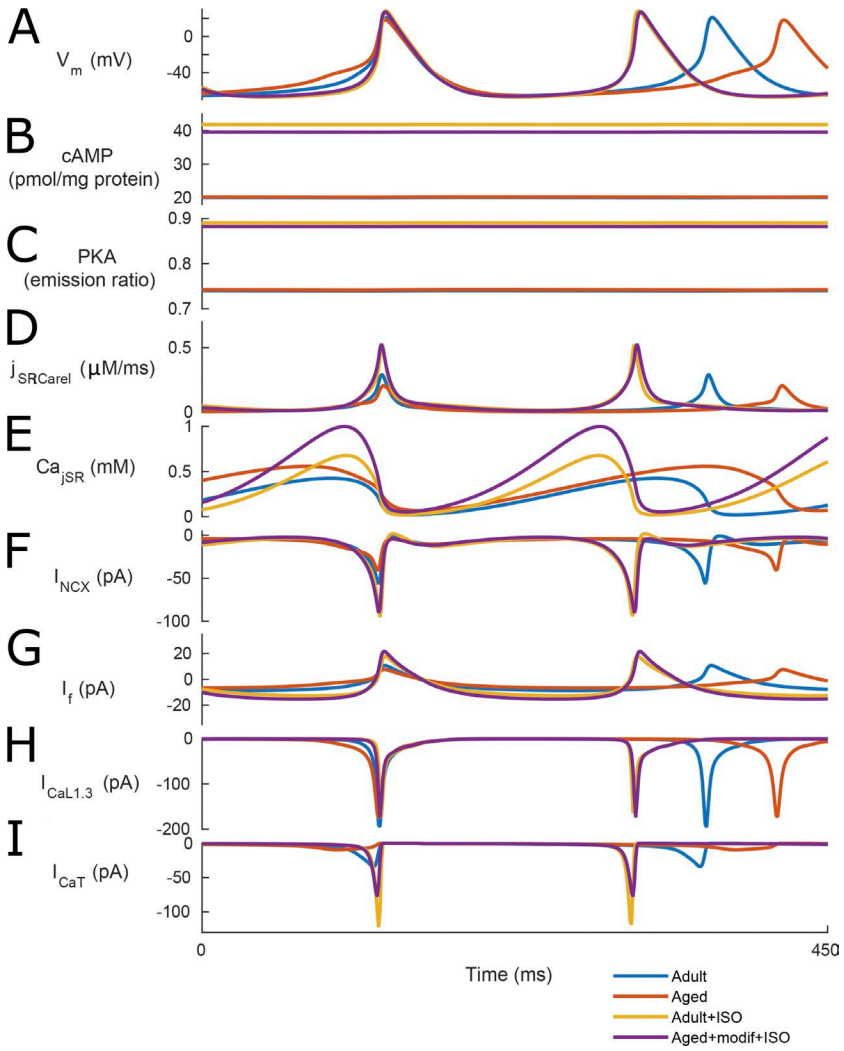

Figure 7. **Model simulation in response to pacemaker function changes occurring in response to ISO in adult and aged mice.** In response to maximal concentration of ISO, AP firing rate (A), cAMP (B), and PKA activities (C) are restored; the flux of Ca^{2+} in the SR ($j_{SRCarel}$; D) and Ca^{2+} concentration in the junctional sarcoplasmic reticulum compartment (Ca_{jSR}; E) are compensated for; and the Na^{+}-Ca^{2+} exchanger current (I_{NCX}; F), HCN current (I_f; G), L-type current (I_{CaL}; H), and T-type Ca^{2+} current (I_{CaT}; I) are completely or partly restored.

clusion is in agreement with experimental data from mouse SAN tissue and pacemaker cells, which have shown deterioration in ionic current (decrease in HCN, L-type, and T-type currents; Larson et al., 2013), Ca^{2+}-related mechanisms (decrease in the amount of RyR and SERCA; Liu et al., 2014), and the node signaling that coupled the clocks (Ca^{2+} global and local release parameters; Liu et al., 2014). Note that only when changes in SERCA, I_f, and RyR (i.e., both M-related and Ca^{2+}-related clock mechanisms) are taken into account can we simulate both the age-associated decrease in basal mean AP firing rate and the changes in other experimentally measured coupled-clock mechanisms (Fig. 1). Because the two clocks are coupled (Yaniv et al., 2013b), changes in one mechanism related to one clock can indirectly affect mechanisms related to the other clock (Behar et al., 2016). Thus, even when changes in only one clock mechanism are taken into account (either M or Ca^{2+} in Fig. 3), the clock entrainment leads to indirect changes in the other. Consequently, an explicit change in the numerical model equations for a specific mechanism is not always necessary to describe known experimental modifications observed in that mechanism's function. For example, the Na^{+}/Ca^{2+} exchanger (NCX) current decreases in aged simulations as a consequence of changes in other mechanisms related to Ca^{2+} signaling (Fig. 3). Importantly, entrainment between the clocks means that restoring one mechanism may partially restore the others; thus, even if a particular drug is not known to restore a specific mechanism, it can restore it indirectly by acting on other mechanisms.

Our second major conclusion is that the sensitivity to β-AR stimulation or PDE inhibition is reduced in advanced age (Fig. 9). These results are in accordance with recently published data (Liu et al., 2014; Yaniv et al., 2016). This reduction in sensitivity can be the result of a reduction in the number of receptors or in the sensitivity of each receptor. Thus, a higher dose of drugs is needed to induce the desired response.

Our third major conclusion is that the reduced maximal beating rate can be reversed using maximal ANS stimulation, cAMP application, or PDE inhibition (Figs. 6, 7, and 8). These results are in accordance with recent publications in which the reduced maximal HR of aged

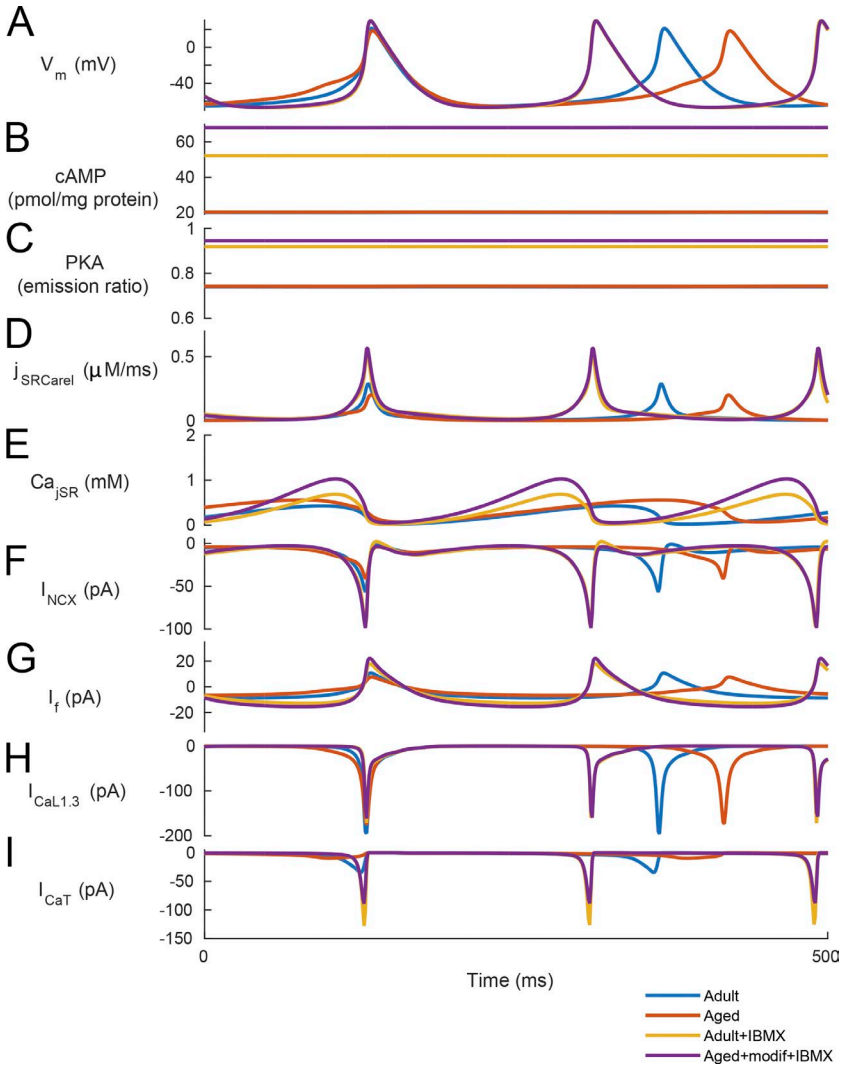

Figure 8. **Model simulation in response to pacemaker function changes occurring in response to IBMX in adult and aged mice.** In response to maximal concentration of IBMX, AP firing rate (A), cAMP (B), and PKA (C) activities are restored; the flux of Ca^{2+} existing the SR ($j_{SRCarel}$; D) and Ca^{2+} concentration in the junctional sarcoplasmic reticulum compartment (Ca_{jSR}; E) are compensated for; and the Na^{+}-Ca^{2+} exchanger current (I_{NCX}; F), HCN current (I_f; G), L-type current (I_{CaL}; H), and T-type Ca^{2+} current (I_{CaT}; I) are completely or partly restored.

pacemaker tissue can be reversed by maximal β-AR stimulation by using ISO or a high level of PDE inhibition using IBMX (Liu et al., 2014; Yaniv et al., 2016). In addition, the maximal AP firing rate could be restored in single isolated pacemaker cells by cAMP (Sharpe et al., 2017). Our model predicts that the age-associated reduction in maximal beating rate can be reversed only if both the relationship between cAMP and HCN_4 and the relationship between PKA and PLB phosphorylation are different in aged mice than in adult mice (Figs. 6, 7, and 8). Our model also predicts that, at maximal β-AR stimulation or PDE inhibition, the cAMP/PKA activity of aged pacemaker tissue is similar to that of adults. It is important to note that restoring the maximal beating rate is not equivalent to reversing the aged cell back to adult cell function because, although the AP firing rate was restored (i.e., the end effect "maximal beating rate"), the intrinsic currents and ion channel conductances are not all the same between adult cells and aged cells that were treated with one of these drugs (Figs. 7 and 8). In other words, a restored maximal beating rate is not equivalent to a restoration of the coupled-clock mechanisms to the adult beating rate but only to its end effect.

Our numerical model equations of the membrane and Ca^{2+} components are in general based on the model of Kharche et al. (2011) (see details in Materials and methods under Basal numerical model). However, to study whether age-deteriorated AP firing is caused by membrane or Ca^{2+} molecules, a description of the node signaling that couples them is critical. Our numerical model is the first to include a description of AC-cAMP-PKA signaling and updated Ca^{2+} dynamics based on recent data (Liu et al., 2014). Thus, only our adaptation to the Kharche et al. (2011) model can be used to answer this study's major question: "What is the relative contribution of each clock to the age-associated deterioration in pacemaker function?" To further elaborate on this question and prove that our conclusions are robust against the choice of the model parameters, we performed parameter sensitivity analysis (Fig. 4). The AP firing rate in the aged model depends on both mem-

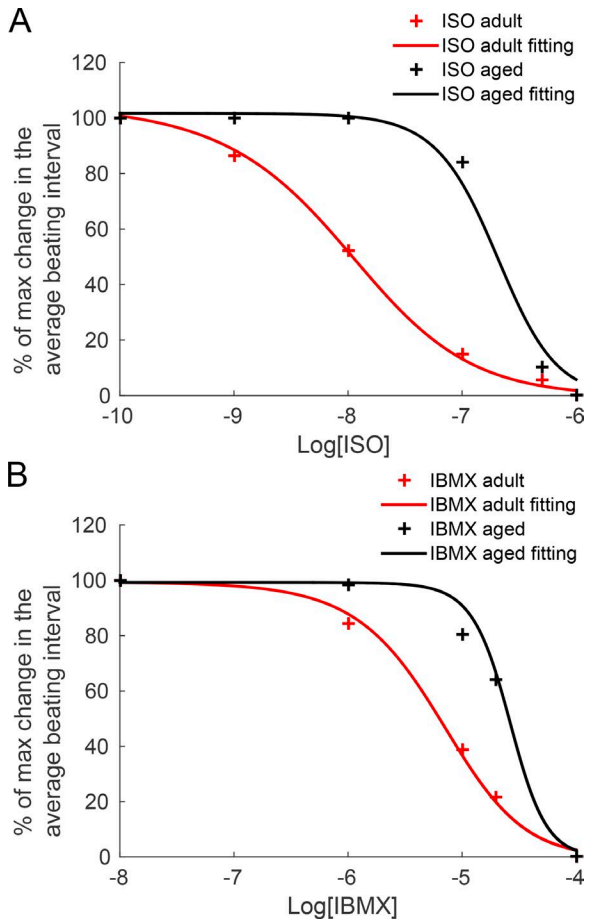

Figure 9. **Age-associated basal AP firing rate can be reversed.** (A) 167 nM ISO can reverse the aged basal AP firing rate to that of adult mouse pacemaker cells. (B) 50 µM IBMX can also reverse the aged basal AP firing rate to that of adult mouse pacemaker cells.

brane and Ca^{2+} clock components when changes in $V_{1/2}$ of the HCN channel or in response to changes in P_{up} of the SERCA are taken into account.

Recent experimental data demonstrate the inability to restore the maximal beating rate of isolated mouse pacemaker cells by means of PDE inhibition (Sharpe et al., 2017). However, these data contradict experimental results at the tissue level (Liu et al., 2014; Yaniv et al., 2016) and our numerical model predictions. Moreover, it is well known that heterogeneity among single SAN cells exists (Boyett et al., 2000) and, importantly, that the heterogeneity of the beating rate increases in the aged model (Lowsky et al., 2014), specifically at the single-cell level (Glauche et al., 2011). Furthermore, during isolation, some receptors and molecules can be impaired, especially in the aged model. Thus, the validity of experiments performed on single cells isolated from a small sample of aged mammals is debatable. To strengthen the findings from single cells, data must also be collected at the SAN tissue level. Note, however, that although pacemaker cell heterogeneity exists in the SAN tissue, the neighborhood effect (Michaels et al., 1986) synchronizes all the cells to follow the strongest one (i.e., the cell that beats the fastest).

Limitations

Our model does not incorporate the previously documented age-associated reduction in the number of NCXs (Liu et al., 2014). Although a decrease in the number of NCXs should result in a lower entrainment level in the coupled-clock model and lead to a decrease in AP firing rate, the numerical model that we used here causes the AP firing rate to increase: reducing the number of NCXs allows more Ca^{2+} to accumulate in the cytosol and thus to increase the AP firing rate. Thus, we did not decrease the conductance of NCX in the numerical model. However, because of the reduction in SERCA, RyR, and HCN channel function, there is

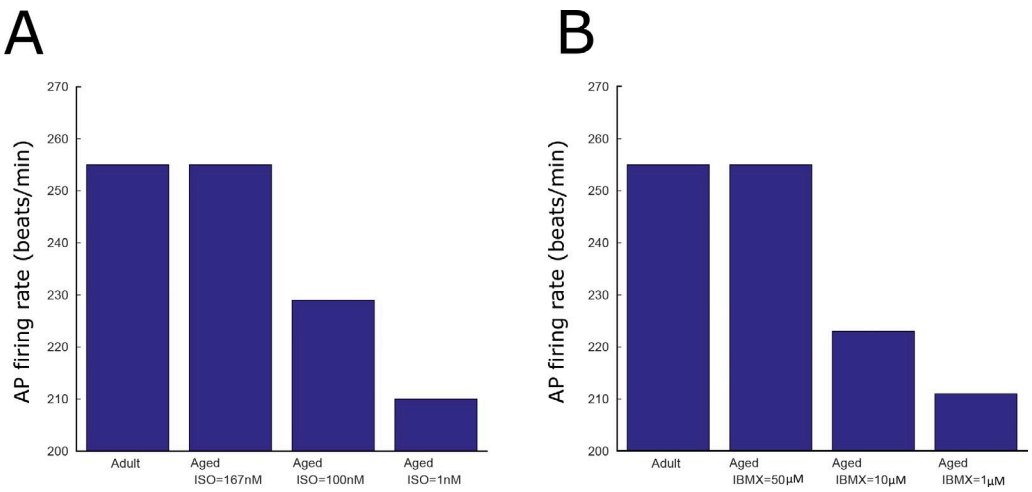

Figure 10. **Sensitivity of AP firing rate to drug perturbations.** (A and B) Simulation of beating interval dynamics in response to PDE inhibition by ISO (A) or IBMX (B).

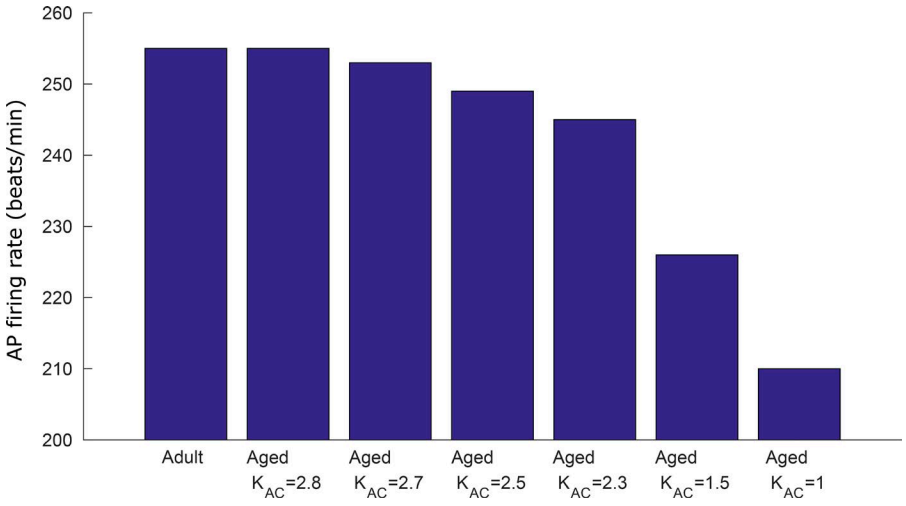

Figure 11. **Overexpression of AC1 or AC8 restores the age-associated reduction in AP firing rate.** Increase in K_{AC} can restore the age-associated reduction in AP firing rate.

a significant decrease in NCX current, which reduces pacemaker function. This is caused by the coupling between the clocks (see above).

Because of the lack of experimental data on Ca^{2+}/calmodulin-dependent protein kinase II (CaMKII) activity in both adult and aged mice (Maltsev et al., 2014; Yaniv and Maltsev, 2014), we did not take into account age-related changes in CaMKII activity. Future experimental data on CaMKII activity in adult and aged pacemaker cells will allow us to explore its function. Moreover, no data exist for both adult and aged mice on local Ca^{2+} concentration and cAMP concentrations. Future experimental data will allow us to develop a local numerical model instead of our common pool model.

We showed in Fig. 6 B that the model predicted an 18% decrease in AP firing rate in aged pacemaker cells. Thus, the model prediction is on the lower bound of the experimental data. This suggests that other mechanisms, although playing a more minor role than the ones modeled, may be involved in further reducing the AP firing rate in aged cells.

The model was designed to describe mouse pacemaker function. Because of its short life span, the mouse is the ideal animal model to explore aging. Thus, the large majority of data on age-deteriorated pacemaker function were reported for mice. However, the end effect of aging in humans and mice is the same: in both models, there is no change in the basal beating rate, but only in the intrinsic beating rate (Jose and Collison, 1970). Future data from SAN tissue and signal pacemaker cells from larger aged mammals, including humans, will make it possible to develop computational models for mammals larger than mice.

The effect of PKA on I_{Ks} was documented in ventricular and atrial myocytes (Sampson et al., 2008). However, because no experimental data exist for sinoatrial cells, it is ambiguous to model PKA effect on I_{Ks}. Therefore, the current numerical model does not include the PKA effect on I_{Ks}.

Clinical aspects

Maintaining the basal heart rate when there is a decrease in the intrinsic beating rate of SAN cells implies that the ANS system must overcompensate for the deteriorated pacemaker function. Chronic stimulation of the β-AR can lead to cardiac hypertrophy and other damage to the heart (Kudej et al., 1997). We showed here that the PDE inhibitor can reverse the age-associated intrinsic beating rate, and thus may be a therapeutic tool if applied specifically only to the SAN area to prevent chronic stimulation of β-AR.

Overexpression of AC1 and/or AC8 has been suggested as a method to restore normal heart rate in the case of bradycardia (Maltsev et al., 2016). We showed here (Fig. 11) that overexpression of Ca^{2+}-activated AC can reverse the age-associated intrinsic beating rate. Thus, our numerical model shows for the first time the feasibility of such an approach for age-associated deficient pacemaker function.

Although we showed here that the maximal intrinsic beating rate can be restored under in vivo conditions, additional mechanisms, such as the preload and afterload, also affect the heart rate. Because the skeletal muscles contribute to the afterload and preload, they, too, affect the heart rate changes. Thus, even if the maximal action potential firing rate can be restored, aging-associated changes in skeletal muscle may prevent the restoration of maximal HR. Moreover, the ability of the heart to reach its maximal rate in response to pharmacological interventions implies that these drugs also restore the energetic balance in the heart (Yaniv et al., 2013a).

ACKNOWLEDGMENTS

The work was supported by the National Natural Science Foundation of China/Israel Science Foundation Joint Research Program, no. 398/14 (Y. Yaniv), the Ministry of Science and Technology, Israel (Y. Yaniv), an Aly-Kaufman Postdoctoral Fellowship (J. Behar), and the Center for Absorption in Science, Ministry of Aliyah and Immigrant Absorption, State of Israel (J. Behar). The funders had no role in study design, data collection and analysis, decision to publish, or preparation of the manuscript.

The authors declare no competing financial interests.

Author contributions: Y. Yaniv and J. Behar conceived and designed the research; J. Behar performed simulations and analyzed the simulated data; J. Behar and Y. Yaniv drafted the manuscript; J. Behar prepared the figures; and J. Behar and Y. Yaniv edited and revised the manuscript and approved the final version.

José D. Faraldo-Gómez served as editor.

Submitted: 19 March 2017
Revised: 22 June 2017
Accepted: 28 July 2017

REFERENCES

Behar, J., and Y. Yaniv. 2016. Dynamics of PKA phosphorylation and gain-of-function in cardiac pacemaker cells: A computational model analysis. *Am. J. Physiol. Circ. Physiol.* 310:H1259–H1266. http://dx.doi.org/10.1152/ajpheart.00076.2016

Behar, J., A. Ganesan, J. Zhang, and Y. Yaniv. 2016. The autonomic nervous system regulates the heart rate through cAMP-PKA dependent and independent coupled-clock pacemaker cell mechanisms. *Front. Physiol.* 7:419. http://dx.doi.org/10.3389/fphys.2016.00419

Boyett, M.R., H. Honjo, and I. Kodama. 2000. The sinoatrial node, a heterogeneous pacemaker structure. *Cardiovasc. Res.* 47:658–687. http://dx.doi.org/10.1016/S0008-6363(00)00135-8

Brodde, O.E., and K. Leineweber. 2004. Autonomic receptor systems in the failing and aging human heart: Similarities and differences. *Eur. J. Pharmacol.* 500:167–176. http://dx.doi.org/10.1016/j.ejphar.2004.07.022

Ferrari, A.U. 2002. Modifications of the cardiovascular system with aging. *Am. J. Geriatr. Cardiol.* 11:30–33. http://dx.doi.org/10.1111/1467-8446.00044-i1

Glauche, I., L. Thielecke, and I. Roeder. 2011. Cellular aging leads to functional heterogeneity of hematopoietic stem cells: A modeling perspective. *Aging Cell.* 10:457–465. http://dx.doi.org/10.1111/j.1474-9726.2011.00692.x

Hagberg, J.M., W.K. Allen, D.R. Seals, B.F. Hurley, A.A. Ehsani, and J.O. Holloszy. 1985. A hemodynamic comparison of young and older endurance athletes during exercise. *J. Appl. Physiol.* 58:2041–2046.

Heath, G.W., J.M. Hagberg, A.A. Ehsani, and J.O. Holloszy. 1981. A physiological comparison of young and older endurance athletes. *J. Appl. Physiol.* 51:634–640.

Jose, A.D., and D. Collison. 1970. The normal range and determinants of the intrinsic heart rate in man. *Cardiovasc. Res.* 4:160–167. http://dx.doi.org/10.1093/cvr/4.2.160

Kharche, S., J. Yu, M. Lei, and H. Zhang. 2011. A mathematical model of action potentials of mouse sinoatrial node cells with molecular bases. *Am. J. Physiol. Circ. Physiol.* 301:H945–H963. http://dx.doi.org/10.1152/ajpheart.00143.2010

Kudej, R.K., M. Iwase, M. Uechi, D.E. Vatner, N. Oka, Y. Ishikawa, R.P. Shannon, S.P. Bishop, and S.F. Vatner. 1997. Effects of chronic β-adrenergic receptor stimulation in mice. *J. Mol. Cell. Cardiol.* 29:2735–2746. http://dx.doi.org/10.1006/jmcc.1997.0508

Kurata, Y., I. Hisatome, S. Imanishi, and T. Shibamoto. 2002. Dynamical description of sinoatrial node pacemaking: Improved mathematical model for primary pacemaker cell. *Am. J. Physiol. Circ. Physiol.* 283:H2074–H2101. http://dx.doi.org/10.1152/ajpheart.00900.2001

Kusumoto, F.M., and N. Goldschlager. 1996. Cardiac pacing. *N. Engl. J. Med.* 334:89–99. http://dx.doi.org/10.1056/NEJM199601113340206

Larson, E.D., J.R. St Clair, W.A. Sumner, R.A. Bannister, C. Proenza, J. Clair, and W.A. Sumner. 2013. Depressed pacemaker activity of sinoatrial node myocytes contributes to the age-dependent decline in maximum heart rate. *Proc. Natl. Acad. Sci. USA.* 110:18011–18016. http://dx.doi.org/10.1073/pnas.1308477110

Liu, J., S. Sirenko, M. Juhaszova, S.J. Sollott, S. Shukla, Y. Yaniv, and E.G. Lakatta. 2014. Age-associated abnormalities of intrinsic automaticity of sinoatrial nodal cells are linked to deficient cAMP-PKA-Ca^{2+} signaling. *Am. J. Physiol. Circ. Physiol.* 306:H1385–H1397. http://dx.doi.org/10.1152/ajpheart.00088.2014

Lowsky, D.J., S.J. Olshansky, J. Bhattacharya, and D.P. Goldman. 2014. Heterogeneity in healthy aging. *J. Gerontol. A Biol. Sci. Med. Sci.* 69:640–649. http://dx.doi.org/10.1093/gerona/glt162

Maltsev, V.A., and E.G. Lakatta. 2009. Synergism of coupled subsarcolemmal Ca2+ clocks and sarcolemmal voltage clocks confers robust and flexible pacemaker function in a novel pacemaker cell model. *Am. J. Physiol. Circ. Physiol.* 296:H594–H615. http://dx.doi.org/10.1152/ajpheart.01118.2008

Maltsev, V.A., Y. Yaniv, A.V. Maltsev, M.D. Stern, and E.G. Lakatta. 2014. Modern perspectives on numerical modeling of cardiac pacemaker cell. *J. Pharmacol. Sci.* 125:6–38. http://dx.doi.org/10.1254/jphs.13R04CR

Maltsev, V., E. Lakatta, I. Zahanich, and S. Sirenko. 2016. Engineered biological pacemakers. US Patent No. 9506032. 29 November 2016.

Michaels, D.C., E.P. Matyas, and J. Jalife. 1986. Dynamic interactions and mutual synchronization of sinoatrial node pacemaker cells. A mathematical model. *Circ. Res.* 58:706–720. http://dx.doi.org/10.1161/01.RES.58.5.706

Ogawa, T., R.J. Spina, W.H. Martin III, W.M. Kohrt, K.B. Schechtman, J.O. Holloszy, and A.A. Ehsani. 1992. Effects of aging, sex, and physical training on cardiovascular responses to exercise. *Circulation.* 86:494–503. http://dx.doi.org/10.1161/01.CIR.86.2.494

Sampson, K.J., C. Terrenoire, D.O. Cervantes, R.A. Kaba, N.S. Peters, and R.S. Kass. 2008. Adrenergic regulation of a key cardiac potassium channel can contribute to atrial fibrillation: Evidence from an I_{Ks} transgenic mouse. *J. Physiol.* 586:627–637. http://dx.doi.org/10.1113/jphysiol.2007.141333

Sharpe, E.J., E.D. Larson, and C. Proenza. 2017. Cyclic AMP reverses the effects of aging on pacemaker activity and If in sinoatrial node myocytes. *J. Gen. Physiol.* 149:237–247. http://dx.doi.org/10.1085/jgp.201611674

Yaniv, Y., and V.A. Maltsev. 2014. Numerical modeling calcium and CaMKII effects in the SA node. *Front. Pharmacol.* 5:58. http://dx.doi.org/10.3389/fphar.2014.00058

Yaniv, Y., M. Juhaszova, and S.J. Sollott. 2013a. Age-related changes of myocardial ATP supply and demand mechanisms. *Trends Endocrinol. Metab.* 24:495–505. http://dx.doi.org/10.1016/j.tem.2013.06.001

Yaniv, Y., S. Sirenko, B.D. Ziman, H.A. Spurgeon, V.A. Maltsev, and E.G. Lakatta. 2013b. New evidence for coupled clock regulation of the normal automaticity of sinoatrial nodal pacemaker cells: Bradycardic effects of ivabradine are linked to suppression of intracellular Ca^{2+} cycling. *J. Mol. Cell. Cardiol.* 62:80–89. http://dx.doi.org/10.1016/j.yjmcc.2013.04.026

Yaniv, Y., A. Ganesan, D. Yang, B.D. Ziman, A.E. Lyashkov, A. Levchenko, J. Zhang, and E.G. Lakatta. 2015a. Real-time relationship between PKA biochemical signal network dynamics and increased action potential firing rate in heart pacemaker cells: Kinetics of PKA activation in heart pacemaker cells. *J. Mol. Cell. Cardiol.* 86:168–178. http://dx.doi.org/10.1016/j.yjmcc.2015.07.024

Yaniv, Y., E.G. Lakatta, and V.A. Maltsev. 2015b. From two competing oscillators to one coupled-clock pacemaker cell system. *Front. Physiol.* 6:28. http://dx.doi.org/10.3389/fphys.2015.00028

Yaniv, Y., I. Ahmet, K. Tsutsui, J. Behar, J.M. Moen, Y. Okamoto, T.R. Guiriba, J. Liu, R. Bychkov, and E.G. Lakatta. 2016. Deterioration of autonomic neuronal receptor signaling and mechanisms intrinsic to heart pacemaker cells contribute to age-associated alterations in heart rate variability in vivo. *Aging Cell.* 15:716–724. http://dx.doi.org/10.1111/acel.12483

SUPPLEMENTAL MATERIAL

Behar and Yaniv, https://doi.org/10.1085/jgp.201711792

Note on the reversal potentials

The reversal potential of a current flowing through an ion specific channel is represented as an equilibrium potential of the relevant ion. However, experimentally it is often found that the reversal potentials of a given current are not equal to (and sometimes very different from) the Nernst equilibrium potential calculated using the extracellular and intracellular ion concentrations. Our model includes three such apparent potentials for I_{CaL}, I_{CaT}, and $I_{Na1.5}$. These values are based on the apparent potentials provided by the parent model of ours, i.e., Kharche et al. (2011), which itself is based on the model of Kurata et al. (2002).

Equations

General

Membrane potential

$$I_f = I_{fNa} + I_{fK}$$

$$I_b = I_{bNa} + I_{bCa} + I_{bK}$$

$$I_{Na} = I_{Na11} + I_{Na15}$$

$$I = I_f + I_{Na} + I_{CaL} + I_{CaT} + I_{Kr} + I_{Ks} + I_{to} + I_{sus} + I_{K1} + I_{st} + I_{NaK} + I_{NCX} + I_b + I_{KACh}$$

$$dV/dt = -(1/C) \cdot I$$

Gating variables

$$dg/dt = (g_\infty - g)/\tau_g,$$

for any gating variable g with steady state g_∞

Reversal potential

$$E_{Na} = E_T \cdot \log([\mathrm{Na}^+]_o/[\mathrm{Na}^+]_i)$$

$$E_K = E_T \cdot \log([\mathrm{K}^+]_o/[\mathrm{K}^+]_i)$$

$$E_{Ks} = E_T \cdot \log\left(\frac{[\mathrm{K}^+]_o + 0.12 \cdot [\mathrm{Na}^+]_o}{[\mathrm{K}^+]_i + 0.12 \cdot [\mathrm{Na}^+]_i}\right)$$

$$E_{Ca} = (E_T/2) \cdot \log\left(\left[\mathrm{Ca}^{2+}\right]_o/\left[\mathrm{Ca}^{2+}\right]_{sub}\right)$$

AC-cAMP PKA signaling

cAMP activity

$$\frac{d[\mathrm{cAMP}]}{dt} = \frac{k_{iso} \cdot [\mathrm{ATP}] + k_1 \cdot [\mathrm{ATP}] - k_2 \cdot [\mathrm{cAMP}] - k_3 \cdot [\mathrm{cAMP}] - k_{cch} \cdot [\mathrm{ATP}]}{60,000}$$

Adult

$$k_{iso} = 0.1599 \cdot \frac{[\mathrm{ISO}]^{0.6238}}{76.5441^{0.6238} + [\mathrm{ISO}]^{0.6238}}$$

$$k_{ibmx,\ adult} = -0.8730 \cdot \frac{[\mathrm{IBMX}]^{0.8395}}{4.0550^{0.8781} + [\mathrm{IBMX}]^{0.8395}} + 1$$

Aged

$$k_{iso} = 0.1434 \cdot \frac{[\mathrm{ISO}]^{2.0704}}{334.2799^{2.0704} + [\mathrm{ISO}]^{2.0704}}$$

$$k_{ibmx,\ aged} = -0.9118 \cdot \frac{[\mathrm{IBMX}]^{0.8781}}{47.6705^{0.8781} + [\mathrm{IBMX}]^{0.8781}} + 1$$

$$k_{cch} = 0.0146 \cdot \frac{[\mathrm{CCh}]^{1.4402}}{51.7331^{1.4402} + [\mathrm{CCh}]^{1.4402}}$$

$$k_1 = K_{AC,I} + \frac{K_{AC}}{1 + \exp\left(\left(K_{Ca} - k_{bCM} \cdot \frac{f_{CMi}}{k_{fCM} \cdot (1 - f_{CMi})}\right) / K_{AC,Ca}\right)}$$

$$k_2 = k_{ibmx} \cdot 265.3512 \cdot \frac{[\mathrm{cAMP}]^{5.7343}}{24.7290^{6.7343} + [\mathrm{cAMP}]^{6.7343}}$$

$$k_3 = k_{PKA} \cdot \frac{[\mathrm{cAMP}]^{(n_{PKA}-1)}}{k_{PKA,cAMP}^{n_{PKA}} + [\mathrm{cAMP}]^{n_{PKA}}}$$

PLB activity

$$\frac{d[\mathrm{PLB_p}]}{dt} = \frac{k_4 \cdot [\mathrm{PKA}] - k_5 \cdot [\mathrm{PLB_p}]}{6,000}$$

$$k_4 = \left(k_{PLB_p} \cdot [\mathrm{PKA}]^{n_{PLB}-1}\right) / \left(k_{PKA,PLB}^{n_{PLB}} + [\mathrm{PKA}]^{n_{PLB}}\right)$$

$$k_5 = k_{PP1} \cdot \frac{[\mathrm{PP1}]}{k_{PP1,PLB} + [\mathrm{PLB_p}]}$$

PKA activity

The explicit cAMP-PKA relationship was adapted from the model of Saucerman et al. (2003). The system of equations was solved algebraically (see plot in Fig. S3).

$$[\mathrm{PKA}] = 2 - [RC] - [ARC] - [A_2RC] - [PKA_{PKI}]$$

$$[A_2R] = [\mathrm{PKA}] + [PKA_{PKI}]$$

$$[A_2RC] = \frac{[\mathrm{PKA}] \times [A_2R]}{0.009}$$

$$[ARC] = 0.008 \cdot [A_2RC] / [\mathrm{cAMP}]$$

$$[PKA_{PKI}] = [PKI_{tot}] \cdot [\mathrm{PKA}] / (0.001 + [\mathrm{PKA}])$$

$$[RC] = 0.008 \cdot \frac{[ARC]}{[\mathrm{cAMP}]}$$

Membrane currents

4-aminopyridine–sensitive currents, $I_{4AP} = I_{to} + I_{sus}$

$$I_{to} = g_{to} \cdot (V_m - E_K) \cdot q \cdot r$$

$$I_{sus} = g_{sus} \cdot (V_m - E_K) \cdot r$$

$$q_\infty = \frac{1}{1 + \exp((V_m + 49.0)/13.0)}$$

$$r_\infty = \frac{1}{1 + \exp(-(V_m - 19.3)/15.0)}$$

$$\tau_q = \frac{\frac{6.06 + 39.102}{0.57 \cdot \exp(-0.08 \cdot (V_m + 44.0)) + 0.065 \cdot \exp(0.1 \cdot (V_m + 45.93))}}{0.67}$$

$$\tau_r = \frac{\frac{2.75 + 14.40516}{1.037 \cdot \exp(0.09 \cdot (V_m + 30.61)) + 0.369 \cdot \exp(-0.12 \cdot (V_m + 23.84))}}{0.303}$$

Ca^{2+} background current, I_{bCa}

$$I_{bCa} = g_{bCa} \cdot (V_m - E_{Ca})$$

K^+ background current, I_{bk}

$$I_{bK} = g_{bK} \cdot (V_m - E_K)$$

Na^+-dependent background current, I_{bNa}

$$I_{bNa} = g_{bNa} \cdot (V_m - E_{Na})$$

L-type Ca^{2+} current, $I_{Ca,L}$

$$b_{CaL} = -0.2152 + 1.6913 \cdot \frac{PKA^{10.0808}}{0.8836^{10.0808} + PKA^{10.0808}}$$

$$I_{CaL12} = g_{CaL12} \cdot (1 + b_{CaL}) \cdot (V_m - E_{CaL}) \cdot d_{L12} \cdot f_{L12} \cdot f_{Ca}$$

$$I_{CaL13} = g_{CaL13} \cdot (1 + b_{CaL}) \cdot (V_m - E_{CaL}) \cdot d_{L13} \cdot f_{L13} \cdot f_{Ca}$$

$$I_{CaL} = I_{CaL12} + I_{CaL13}$$

$$d_{\infty 12} = \frac{1}{1 + \exp\left(-\frac{V_m + 3.0}{5.0}\right)}$$

$$f_{\infty 12} = \frac{1}{1 + \exp\left(\frac{V_m + 36.0}{4.6}\right)}$$

$$d_{\infty 13} = \frac{1}{1 + \exp\left(-\frac{V_m + 13.5}{6}\right)}$$

$$f_{\infty 13} = \frac{1}{1 + \exp\left(\frac{V_m + 35.0}{7.3}\right)}$$

$$f_{Ca\infty} = \frac{K_{mfCa}}{K_{mfCa} + \mathrm{Ca}_{sub}}$$

$$\alpha_{dL} = -28.39 \cdot \frac{V_m + 35}{\exp\left(-\frac{V_m + 35}{2.5}\right) - 1} - 84.9 \cdot \frac{V_m}{\exp(-0.208 \cdot V_m) - 1}$$

$$\beta_{dL} = \frac{11.43 \cdot (V_m - 5.0)}{\exp(0.4 \cdot (V_m - 5.0)) - 1}$$

$$\tau_{dL} = \frac{2,000}{\alpha_{dL} + \beta_{dL}}$$

$$\tau_{fl} = 7.4 + 45.77 \cdot \exp\left(\frac{-0.5 \cdot (V_m + 28.1) \cdot (V_m + 28.1)}{11 \cdot 11}\right)$$

$$\tau_{fCa} = \frac{f_{Ca\infty}}{\alpha_{fCa}}$$

T-type Ca^{2+} current, I_{CaT}

The conductance of I_{CaT} was decreased by 20% to simulate the current density reduction during DD found in (Larson et al., 2013).

Adult

$$I_{CaT} = g_{CaT} \cdot (V_m - E_{CaT}) \cdot d_T \cdot f_T$$

Aged

$$I_{CaT} = 0.8 \cdot g_{CaT} \cdot (V_m - E_{CaT}) \cdot d_T \cdot f_T$$

$$d_{T\infty} = \frac{1}{1 + \exp\left(-\frac{V_m + 26}{6}\right)}$$

$$f_{T\infty} = \frac{1}{1 + \exp\left(\frac{V_m + 61.7}{5.6}\right)}$$

$$\tau_{dT} = \frac{1}{1.068 \cdot \exp\left(\frac{V_m + 26.3}{30}\right) + 1.068 \cdot \exp\left(-\frac{V_m + 26.3}{30}\right)}$$

$$\tau_{fT} = \frac{1}{0.0153 \cdot \exp\left(-\frac{V_m + 61.7}{83.3}\right) + 0.015 \cdot \exp\left(\frac{V_m + 61.7}{15.38}\right)}$$

Hyperpolarization activated "funny" current, I_f

$V_{0.5}$ was changed in the I_f equation from 104.2 to 110 mV (Larson et al., 2013). In addition, the expression for V_{shift} was modified in the aged model (Fig. S2) to match the maximal increase in V_{shift} found experimentally in Larson et al. (2013).

$$I_{fNa} = 0.3833 \cdot g_{If} \cdot (V_m - E_{Na}) \cdot y$$

$$I_{fK} = 0.6167 \cdot g_{If} \cdot (V_m - E_K) \cdot y$$

Adult

$$K_{if} = 25.3403, \quad K_{0.5if} = 18.1115, \quad n_{if} = 9.6383$$

$$V_{shift} = \frac{K_{if} \cdot [\text{cAMP}]^{n_{if}}}{\left(K_{0.5if}{}^{n_{if}} + [\text{cAMP}]^{n_{if}}\right)} - 18.1040$$

$$y_\infty = \frac{1}{1 + \exp\left(\frac{V_m + 104.2 - V_{shift}}{16.3}\right)}$$

Aged

$$K_{if} = 35.7355, \quad K_{0.5if} = 19.9587, \quad n_{if} = 9.6383$$

$$V_{shift} = \frac{K_{if} \cdot [\text{cAMP}]^{n_{if}}}{\left(K_{0.5if}{}^{n_{if}} + [\text{cAMP}]^{n_{if}}\right)} - 35$$

$$y_\infty = \frac{1}{1 + \exp\left(\frac{V_m + 110 - V_{shift}}{16.3}\right)}$$

$$\tau_y = \frac{1.5049}{\exp(-(V_m + 590.3) \cdot 0.01094) + \exp\left(\frac{V_m - 85.1}{17.2}\right)}$$

Inward rectifier current, I_{k1}

$$I_{K1} = g_{K1} \cdot \frac{1}{1 + \exp(0.070727 \cdot (V_m - E_K))} \cdot \frac{K_0}{([K^+]_o + 0.228880)} \cdot (V_m - E_K)$$

Rapidly activating delayed rectifier K^+ current, I_{Kr}

$$I_{Kr} = g_{Kr} \cdot (V_m - E_K) \cdot p_a \cdot p_i$$

$$p_{a\infty} = \frac{1}{1 + \exp\left(-\frac{V_m + 21.173694}{9.757086}\right)}$$

$$p_{i\infty} = \frac{1}{1+\exp\left(\frac{V_m+20.758474-4.0}{19.0}\right)}$$

$$\tau_{pa} = \frac{0.699821}{0.003596\cdot\exp\left(\frac{V_m}{15.339290}\right)+0.000177\cdot\exp\left(\frac{-V_m}{25.868423}\right)}$$

$$\tau_{pi} = 0.2+\frac{0.9\cdot 1.0}{0.1\cdot\exp\left(\frac{V_m}{54.645}\right)+0.656\cdot\exp\left(\frac{V_m}{106.157}\right)}$$

Slow activating delayed rectifier K^+ current, I_{Ks}

$$I_{Ks} = g_{Ks}\cdot(V_m-E_{Ks})\cdot xs^2$$

$$xs_\infty = \frac{1}{1+\exp\left(-\frac{V_m-20.876040}{11.852723}\right)}$$

$$\tau_{xs} = \frac{1,000}{\frac{13.097938}{1+\exp\left(-\frac{V_m-48.910584}{10.630272}\right)}+\exp\left(-\frac{V_m}{35.316539}\right)}$$

Sodium currents, I_{Na11} and I_{Na15}

$$FNa = \frac{(9.52\cdot 10^{-2})\cdot\exp((-6.3\cdot 10^{-2})\cdot(V_m+34.4))}{1+1.66\cdot\exp(-0.225\cdot(V_m+63.7))+(8.69\cdot 10^{-2})}$$

$$hs_{11} = (1-FNa)\cdot h11+FNa\cdot j11 \quad hs_{15} = (1-FNa)\cdot h15+FNa\cdot j15$$

$$I_{Na11} = g_{Na11}\cdot m_{11}^3\cdot hs_{11}\cdot V_m\cdot[\mathrm{Na}]_0\cdot\frac{F}{E_T\cdot 1,000}\cdot\frac{\exp((V_m-\mathrm{E}_{Na})/E_T)-1}{\exp(V_m/E_T)-1}$$

$$I_{Na15} = g_{Na15}\cdot m_{15}^3\cdot hs_{15}\cdot V_m\cdot[\mathrm{Na}]_0\cdot\frac{F}{E_T\cdot 1,000}\cdot\frac{\exp((V_m-E_{\mathrm{Na}15})/E_T)-1}{\exp(V_m/E_T)-1}$$

$$I_{Na} = I_{Na11}+I_{Na15}$$

$$m_{11,\infty} = \frac{1}{1+\exp\left(\frac{-(V_m+36.097331-5.0)}{5.0}\right)^{1/3}}$$

$$h_{11,\infty} = \frac{1}{1+\exp\left(\frac{V_m+56.0}{3.0}\right)}$$

$$j_{11,\infty} = h_{11,\infty}$$

$$m_{15,\infty} = \frac{1}{1+\exp\left(\frac{-(V_m+45.213705)}{7.219547}\right)^{1/3}}$$

$$h_{15,\infty} = \frac{1}{1+\exp\left(\frac{-(V_m+62.578120)}{-6.084036}\right)}$$

$$j_{15,\infty} = h_{15,\infty}$$

$$\tau_{m11} = \frac{1,000\cdot(0.6247\cdot 10^{-3})}{0.832\cdot\exp(-0.335\cdot(V_m+56.7))+0.627\cdot\exp(0.082\cdot(V_m+65.01))}+0.0000492$$

$$\tau_{h11} = \frac{1,000.0\cdot(3.717\cdot 10^{-6})\cdot\exp(-0.2815\cdot(V_m+17.11))}{1+0.003732\cdot\exp(-0.3426\cdot(V_m+37.76))}+0.0005977$$

$$\tau_{j11} = \frac{1,000\cdot(0.00000003186\cdot\exp(-0.6219\cdot(V_m+18.8)))}{1+0.00007189\cdot\exp(-0.6683\cdot(V_m+34.07))}+0.003556)$$

$$\tau_{m15} = \tau_{m11}$$

$$\tau_{h15} = \tau_{h11}$$

$$\tau_{j15} = \tau_{j11}$$

Na^+-K^+ pump current, I_{NaK}

$$I_{NaK} = I_{NaKmax} \cdot \frac{\frac{([K^+]_o)^{1.2}}{(K_{mK})^{1.2} + ([K^+]_o)^{1.2}} \cdot \frac{([Na^+]_i)^{1.3}}{(K_{mNa})^{1.3} + ([Na^+]_i)^{1.3}}}{1.0 + \exp\left(\frac{-(V_m - E_{Na} + 120)}{30}\right)}$$

Na^+-Ca^{2+} exchanger current, I_{NCX}

$$d_0 = 1 + \frac{[Ca^{2+}]_o}{K_{co}} \cdot \left(1 + \exp\left(\frac{Q_o \times V_m}{E_T}\right)\right) + \frac{[Na^+]_o}{K_{1no}} \cdot \left(1 + \frac{[Na^+]_o}{K_{2no}} \cdot \frac{1 + [Na^+]_o}{K_{3no}}\right)$$

$$k_{43} = \frac{[Na^+]_i}{K_{3ni} + [Na^+]_i}$$

$$k_{41} = \exp\left(\frac{-Q_n \cdot V_m}{2 \cdot E_T}\right)$$

$$k_{34} = \frac{[Na^+]_o}{K_{3no} + [Na^+]_o}$$

$$k_{21} = \frac{[Ca^{2+}]_o}{K_{co}} \cdot \exp\left(\frac{Q_{co} \cdot V_m}{E_T}\right) / d_0$$

$$k_{23} = \frac{[Na^+]_o}{K_{1no}} \cdot \frac{[Na^+]_o}{K_{2no}} \cdot \frac{1 + [Na^+]_o}{K_{3no}} \cdot \exp\left(\frac{-Q_n \cdot V_m}{2 \cdot E_T}\right) / d_0$$

$$k_{32} = \exp\left(Q_n \cdot \frac{V_m}{2 \cdot E_T}\right)$$

$$x_1 = k_{34} \cdot k_{41} \cdot (k_{23} + k_{21}) + k_{21} \cdot k_{32} \cdot (k_{43} + k_{41})$$

$$d_i = 1 + \frac{[Ca^{2+}]_{sub}}{K_{ci}} \cdot \left(\frac{1 + \exp\left(\frac{-Q_{ci} \cdot V_m}{E_T}\right) + [Na^+]_i}{K_{cni}}\right) + \frac{[Na^+]_i}{K_{1ni}} \cdot \left(1 + \frac{[Na^+]_i}{K_{2ni}} \cdot \frac{1 + [Na^+]_i}{K_{3ni}}\right)$$

$$k_{12} = \frac{[Ca^{2+}]_{sub}}{K_{ci}} \cdot \exp\left(\frac{-Q_{ci} \cdot V_m}{E_T}\right) / d_i$$

$$k_{14} = \frac{[Na^+]_i}{K_{1ni}} \cdot \frac{[Na^+]_i}{K_{2ni}} \cdot \frac{1 + [Na^+]_i}{K_{3ni}} \cdot \exp\left(\frac{Q_n \cdot V_m}{2 \cdot E_T}\right) / d_i$$

$$x_2 = k_{43} \cdot k_{32} \cdot (k_{14} + k_{12}) + k_{41} \cdot k_{12} \cdot (k_{34} + k_{32})$$

$$x_3 = k_{43} \cdot k_{14} \cdot (k_{23} + k_{21}) + k_{12} \cdot k_{23} \cdot (k_{43} + k_{41})$$

$$x_4 = k_{34} \cdot k_{23} \cdot (k_{14} + k_{12}) + k_{21} \cdot k_{14} \cdot (k_{34} + k_{32})$$

$$I_{NCX} = K_{NaCa} \cdot \frac{k_{21} \cdot x_2 - k_{12} \cdot x_1}{x_1 + x_2 + x_3 + x_4}$$

Acetylcholine-activated K^+ current, I_{KACh}

The formulation of the current is based on the original work of Demir et al. (1999) and its further modification in Maltsev and Lakatta (2010):

$$I_{KACh} = C_m \cdot g_{KACh} \cdot w \cdot (V_m - E_K)$$

$$\beta_w = 0.001 \cdot \frac{12.32}{1 + (0.0042/[\mathrm{CCh}] \cdot 10^{-6})}$$

$$\alpha_w = 0.001 \cdot 17 \cdot \exp(0.0133 \cdot (V_m + 40))$$

$$w_\infty = \frac{\beta_w}{\alpha_w + \beta_w}$$

$$\tau_w = \frac{1}{\alpha_w + \beta_w}$$

Sarcoplasmic reticulum Ca^{2+} cycling

RyR function

Adult

$$j_{SRCarel} = k_s \cdot OO \cdot \left(\left[\mathrm{Ca}^{2+}\right]_{\mathrm{jSR}} - \left[\mathrm{Ca}^{2+}\right]_{\mathrm{sub}} \right)$$

Aging

$$j_{SRCarel} = 0.35 \cdot k_s \cdot OO \cdot \left(\left[\mathrm{Ca}^{2+}\right]_{\mathrm{jSR}} - \left[\mathrm{Ca}^{2+}\right]_{\mathrm{sub}} \right)$$

$$k_{CaSR} = MaxSR - \frac{MaxSR - MinSR}{1 + \left(EC_{50SR} / \left[\mathrm{Ca}^{2+}\right]_{\mathrm{jSR}}\right)^{HSR}}$$

$$k_{oSRCa} = \frac{k_{oCa}}{k_{CaSR}}$$

$$k_{iSRCa} = k_{iCa} \cdot k_{CaSR}$$

$$\frac{dR}{dt} = \left(k_{im} \cdot RI - k_{iSRCa} \cdot \left[\mathrm{Ca}^{2+}\right]_{\mathrm{sub}} \cdot R\right) - \left(k_{oSRCa} \cdot \left[\mathrm{Ca}^{2+}\right]_{\mathrm{sub}}^2 \cdot R - k_{om} \cdot OO\right)$$

$$\frac{dOO}{dt} = \left(k_{oSRCa} \cdot \left[\mathrm{Ca}^{2+}\right]_{\mathrm{sub}}^2 \cdot R - k_{om} \cdot OO\right) - \left(k_{iSRCa} \cdot \left[\mathrm{Ca}^{2+}\right]_{\mathrm{sub}} \cdot OO - k_{im} \cdot S\right)$$

$$\frac{dS}{dt} = \left(k_{iSRCa} \cdot \left[\mathrm{Ca}^{2+}\right]_{\mathrm{sub}} \cdot OO - k_{im} \cdot S\right) - \left(k_{om} \cdot S - k_{oSRCa} \cdot \left[\mathrm{Ca}^{2+}\right]_{\mathrm{sub}}^2 \cdot RI\right)$$

$$\frac{dRI}{dt} = \left(k_{om} \cdot S - k_{oSRCa} \cdot \left[\mathrm{Ca}^{2+}\right]_{\mathrm{sub}}^2 \cdot RI\right) - \left(k_{im} \cdot RI - k_{iSRCa} \cdot \left[\mathrm{Ca}^{2+}\right]_{\mathrm{sub}} \cdot R\right)$$

The rate of Ca^{2+} uptake (pumping) by the SR, j_{up}

The formulation of the equation is based on the model of Luo and Rudy (1994) and modified to take into account the modulation of the SERCA pump by PLB_p. In aged cells, SERCA activity is decreased by 30%, as observed experimentally in Liu et al. (2014).

Adult

$$f\left(\left[\mathrm{PLB_p}\right]\right) = 2.9102 \cdot \frac{\left[\mathrm{PLB_p}\right]^{9.5517}}{0.2763^{9.5517} + \left[\mathrm{PLB_p}\right]^{9.5517}} + 0.4998$$

$$j_{up} = P_{up} \cdot \frac{f\left(\left[\mathrm{PLB_p}\right]\right)}{\frac{1 + K_{up}}{\left[\mathrm{Ca}^{2+}\right]_{\mathrm{i}}}}$$

Aged

$$f\left(\left[PLB_p\right]\right) = 4.0152 \cdot \frac{\left[\mathrm{PLB_p}\right]^{9.9463}}{0.2853^{9.9463} + \left[\mathrm{PLB_p}\right]^{9.9463}} + 0.4999$$

$$j_{up} = 0.7 \cdot P_{up} \cdot \frac{f\left(\left[PLB_p\right]\right)}{\frac{1 + K_{up}}{\left[\mathrm{Ca}^{2+}\right]_{\mathrm{i}}}}$$

Ca^{2+} diffusion flux from submembrane space to myoplasm, $j_{Ca,dif}$

$$j_{Cadiff} = \frac{\left[Ca^{2+}\right]_{sub} - \left[Ca^{2+}\right]_i}{\tau_{difCa}}$$

Ca^{2+} flux between network and junctional SR compartments, j_{tr}

$$j_{tr} = \frac{\left[Ca^{2+}\right]_{nSR} - \left[Ca^{2+}\right]_{jSR}}{\tau_{diftr}}$$

Natural Ca^{2+} buffering

$$df_{TC} = f_{kl} \cdot \left[Ca^{2+}\right]_i \cdot (1 - A - TT) - k_l \cdot (A + TT)$$

$$df_{TMC} = k_{fTMC} \cdot \left[Ca^{2+}\right]_i \cdot (1 - f_{TMC} - f_{TMM}) - k_{bTMC} \cdot f_{TMC}$$

$$df_{TMM} = k_{fTMM} \cdot \left[Mg^{2+}\right]_i \cdot (1 - f_{TMC} - f_{TMM}) - k_{bTMM} \cdot f_{TMM}$$

$$df_{CMi} = k_{fCM} \cdot \left[Ca^{2+}\right]_i \cdot (1 - f_{CMi}) - k_{bCM} \cdot f_{CMi}$$

$$df_{CMs} = k_{fCM} \cdot \left[Ca^{2+}\right]_{sub} \cdot (1 - f_{CMs}) - k_{bCM} \cdot f_{CMs}$$

$$df_{CQ} = k_{fCQ} \cdot \left[Ca^{2+}\right]_{jSR} \cdot (1 - f_{CQ}) - k_{bCQ} \cdot f_{CQ}$$

Dynamics of Ca^{2+} concentrations in cell compartments

$$\frac{d\left[Ca^{2+}\right]_i}{dt} = \frac{j_{Cadif} \cdot V_{sub} - j_{up} \cdot V_{nSR}}{V_i} - \left(CM_{tot} \cdot \frac{df_{CMi}}{dt} + TC_{tot} \cdot \frac{df_{TC}}{dt} + TMC_{tot} \cdot \frac{df_{TMC}}{dt} \right)$$

$$\frac{d\left[Ca^{2+}\right]_{sub}}{d} = \frac{\frac{-(I_{CaL} + I_{CaT} + I_{bCa} - 2 \cdot I_{NCX})}{\frac{2 \times F}{1,000}} + j_{SRCarel} \cdot V_{jSR}}{V_{sub} - j_{Cadiff} - CM_{tot} \cdot df_{CMs}}$$

$$\frac{d\left[Ca^{2+}\right]_{jSR}}{dt} = j_{tr} - j_{SRCarel} - CQ_{tot} \cdot df_{CQ}$$

$$\frac{d\left[Ca^{2+}\right]_{nSR}}{dt} = \frac{j_{up} - j_{tr} \cdot V_{jSR}}{V_{nSR}}$$

Force

The force model parameters are based on the Yaniv–Landesberg model (Yaniv et al., 2005), and N_c and F_{XB} were fitted based on the experimental results of Catanzaro et al. (2006).

$$\frac{dSL}{dt} = -V_e$$

$$N_{XB} = \frac{(SL - SL_0) \cdot N_c \cdot (TT - U) \cdot 1,000}{2}$$

$$K_{Ca} = \frac{F_{ko} + F_{k1} \cdot N_{XB}^{FN}}{F_{k0.5}^{FN} + N_{XB}^{FN}}$$

$$k_{-1} = \frac{F_{kl}}{K_{Ca}}$$

$$\frac{dA}{dt} = F_{kl} \cdot \left[Ca^{2+}\right]_i \cdot (1 - A - TT - U) - A \cdot (F_f + k_{-l}) + TT \cdot (F_{go} - F_{gl} \cdot V_e)$$

$$\frac{dTT}{dt} = F_f \cdot A - TT \cdot (F_{g0} + F_{g1} \cdot V_e + k_{-l}) + F_{kl} \cdot \left[Ca^{2+}\right]_i \cdot U$$

$$\frac{dU}{dt} = k_{-l} \cdot TT - (F_{g0} + F_{g1} \cdot V_e + F_{kl} \cdot \left[Ca^{2+}\right]_i) \cdot U$$

$$\frac{dV_e}{dt} = 0$$

ATP-ADP

The equations were taken from Yaniv et al. (2015).

$$ATP_i = ATP_{i,max} \cdot \left(\frac{k_{ATP} \cdot \left(\frac{[\text{cAMP}]}{cAMPb} \right)^{n_{ATP}}}{k_{ATP,0.5} + \left(\frac{[\text{cAMP}]}{cAMPb} \right)^{n_{ATP}}} - K_{ATP,min} \right)$$

Table S1. **Coupled differential equation variables: Initial conditions**

No.	Model parameter	Units	Value	Definition
1	V_m	mV	−64.521628694	Membrane potential
2	d_T		0.0016256324	Inactivation gate for I_{CaT}
3	f_T		0.4264459666	Activation gate for I_{CaT}
4	p_a		0.4043600437	Activation gating variable for I_{Kr}
5	p_i		0.9250035423	Inactivation gating variable for I_{Kr}
6	x_s		0.0127086259	Activation gating variable for I_{Ks}
7	$f_{L,1.2}$		0.9968141226	Inactivation gate for $I_{CaL,1.2}$
8	$d_{L,1.2}$		0.0000045583	Activation gate for $I_{CaL,1.2}$
9	$f_{L,1.3}$		0.9809298233	Inactivation gate for $I_{CaL,1.3}$
10	$d_{L,1.3}$		0.0002036671	Activation gate for $I_{CaL,1.3}$
11	f_{Ca}		0.7649576191	Ca^{2+}-dependent inactivation gating variable for $I_{CaL,1.2}$ and $I_{CaL,1.3}$
12	r		0.0046263658	Activation gating variable for I_{to} and I_{sus}
13	q		0.6107148187	Inactivation gating variable for I_{to}
14	$m_{1.5}$		0.4014088304	Activation gating variable for Nav1.5
15	$h_{1.5}$		0.2724817537	Fast inactivation gating variable for Nav1.5
16	$j_{1.5}$		0.0249208708	Slow inactivation gating variable for Nav1.5
17	$m_{1.1}$		0.1079085266	Activation gating variable for Nav1.1
18	$h_{1.1}$		0.4500098710	Fast inactivation gating variable for Nav1.1
19	$j_{1.1.}$		0.0268486392	Slow inactivation gating variable for Nav1.1
20	y		0.0279984462	Activation gating variable for I_f
21	$[Ca^{2+}]_i$	mM	0.0000319121	Intracellular Ca^{2+} concentration or Ca^{2+} concentration in the cytosol
22	$[Ca^{2+}]_{jSR}$	mM	0.1187281829	Ca^{2+} concentration in the junctional SR
23	$[Ca^{2+}]_{nSR}$	mM	1.5768287365	Ca^{2+} concentration in the network SR
24	$[Ca^{2+}]_{sub}$	mM	0.0000560497	Ca^{2+} concentration in the subspace
25	f_{TC}		0.0063427103	Fractional occupancy of the troponin Ca^{2+} site by $[Ca^{2+}]_i$
26	f_{TMC}		0.1296677919	Fractional occupancy of the troponin Mg^{2+} site by $[Ca^{2+}]_i$
27	f_{TMM}		0.7688656371	Fractional occupancy of the troponin Mg^{2+} site by Mg^{2+}
28	f_{CMs}		0.0242054739	Fractional occupancy of calmodulin by $[Ca^{2+}]_{sub}$
29	f_{CMi}		0.0138533048	Fractional occupancy of calmodulin by $[Ca^{2+}]_i$
30	f_{CQ}		0.1203184861	Fractional occupancy of calsequestrin by $[Ca^{2+}]_{rel}$
31	R		0.7720290515	Fraction of reactivated (closed) RyR channels
32	OO		0.0000000760	Open fraction of RyR channels
33	S		0.0000000213	Inactive fraction of RyR channels
34	RI		0.2162168926	Fraction of RyR inactivated channels
35	W		0.0004	I_{KACh} ACh and voltage-dependent gating variable
36	[cAMP]	pmol/mg protein	19.73	cAMP
37	[PLB]		0.23	PLB phosphorylation level
38	A		0.06	Density of regulatory units with bound Ca^{2+} and adjacent weak cross-bridges
39	TT		0.02	Density of regulatory units with bound Ca^{2+} and adjacent strong cross-bridge
40	U		0.06	Density of regulatory units without bound but with adjacent strong cross-bridge
41	SL	μm	1.75×10^{-6}	Sarcomere length

Table S2. **Model constants**

Model parameter	Units	Value	Definition
Ion concentration			
$[Mg^{2+}]_i$	mM	2.5	Intracellular Mg^{2+} concentration
$[Na^+]_o$	mM	140	Extracellular Na^+ concentration
$[Ca^{2+}]_o$	mM	2	Extracellular Ca^{2+} concentration
$[K^+]_o$	mM	5.4	Extracellular K^+ concentration
$[Na^+]_i$	mM	10	Intracellular Na^+ concentration
$[K^+]_i$	mM	139.8854603066	Intracellular K^+ concentration
Cell compartments in the numerical model			
C	pF	25	Cell electric capacitance
V_{cell}	pL	3	Cell volume
V_{sub}	pL	0.03328117	Subspace volume
V_{jSR}	pL	0.0036	Volume of the junctional SR
V_i	pL	1.34671883	Myoplasmic volume
V_{nSR}	pL	0.0348	Volume of network SR (Ca^{2+} uptake store)
F	C/M	96485	Faraday constant
T	K	310.5	Absolute temperature for 37°C
R	J/(MK)	8.314472	Universal gas constant
E_{CaL}	mV	47	Reversal potential of I_{CaL}
E_{Na15}	mV	41.5761	Reversal potential of I_{Na15}
E_{CaT}	mV	45	Reversal potential of I_{CaT}
E_T	mV	$1{,}000 \times (R \times T/F)$	
Na^+/Ca^{2+} exchanger current parameters			
K_{1ni}	mM	395.3	Dissociation constant for $[Na^+]_i$ binding to the first site on I_{NCX} transporter
K_{1no}	mM	1,628	Dissociation constant for $[Na^+]_o$ binding to first site on I_{NCX} transporter
K_{2ni}	mM	2.289	Dissociation constant for $[Na^+]_i$ binding to second site on I_{NCX} transporter
K_{2no}	mM	561.4	Dissociation constant for $[Na^+]_o$ binding to second site on I_{NCX} transporter
K_{3ni}	mM	26.44	Dissociation constant for $[Na^+]_i$ binding to third site on I_{NCX} transporter
K_{3no}	mM	4.663	Dissociation constant for $[Na^+]_o$ binding to third site on I_{NCX} transporter
K_{ci}	mM	0.0207	Dissociation constant for $[Na^+]_o$ binding to I_{NCX} transporter
K_{co}	mM	3.663	Dissociation constant for $[Na^+]_o$ binding to I_{NCX} transporter
K_{cni}	mM	26.44	Dissociation constant for $[Na^+]_i$ and $[Ca^{2+}]_i$ simultaneous binding to I_{NCX} transporter
Q_{ci}		0.1369	Fractional charge movement during the $[Ca^{2+}]_{sub}$ occlusion reaction of the I_{NCX} transporter
Q_{co}		0	Fractional charge movement during the $[Ca^{2+}]_o$ occlusion reaction of the I_{NCX} transporter
Q_n		0.4315	Fractional charge movement during Na^+ occlusion reaction of the I_{NCX} transporter
Ca^{2+} flux parameters			
τ_{difCa}	ms	0.04	Time constant of Ca^{2+} diffusion from the submembrane to myoplasm
TC_{tot}	mM	0.031	Total concentration of the troponin-Ca^{2+} site
TMC_{tot}	mM	0.062	Total concentration of the troponin-Mg^{2+} site
k_{fTC}	$mM^{-1}{\cdot}ms^{-1}$	88.8	Ca^{2+} association constant of troponin
k_{fTMC}	$mM^{-1}{\cdot}ms^{-1}$	237.7	Ca^{2+} association constant for the troponin-Mg site
k_{bTC}	ms^{-1}	0.446	Ca^{2+} dissociation constant for the troponin-Ca site
k_{bTMC}	ms^{-1}	0.00751	Ca^{2+} dissociation constant for the troponin-Mg site
k_{fTMM}	$mM^{-1}{\cdot}ms^{-1}$	2.277	Mg^{2+} association constant for the troponin-Mg site
k_{bTMM}	ms^{-1}	0.751	Mg^{2+} dissociation constant for the troponin-Mg site
CM_{tot}	mM	0.045	Total calmodium concentration
k_{fCM}	$mM^{-1}{\cdot}ms^{-1}$	227.7	Ca^{2+} association constant for calsequestrin
k_{bCM}	ms^{-1}	0.542	Ca^{2+} dissociation constant for calmodulin
CQ_{tot}	mM	10	Total calsequestrin concentration
k_{fCQ}	$mM^{-1}{\cdot}ms^{-1}$	0.534	Ca^{2+} association constant for calsequestrin
k_{bCQ}	1/ms	0.445	Dissociation constant for calsequestrin
k_{oCa}	$1/(mM^2{\cdot}ms)$	10	Baseline non–SR-dependent transition rate constant for RyR
k_{om}	ms^{-1}	0.06	Rate transition constant for RyR
k_{iCa}	$mM^{-1}{\cdot}ms^{-1}$	0.5	RyR Ca^{2+} dependent inactivation rate
k_{im}	ms^{-1}	0.005	Rate transition constant for RyR
EC_{50SR}	mM	0.45	EC_{50} for Ca^{2+} SR-dependent activation of SR Ca^{2+} release
MaxSR		15	Ca^{2+} modeling parameter
MinSR		1	Ca^{2+} modeling parameter
HSR		2.5	Parameter for Ca^{2+}-dependent activation of SR Ca^{2+} release
n_{up}		2	SR Ca^{2+} uptake and Hill coefficient
P_{up}	mM/ms	0.02	Rate constant for Ca^{2+} uptake by the Ca^{2+} pump in the network SR
k_s	ms^{-1}	250×10^3	Release rate parameter

Table S2. **Model constants** *(Continued)*

Model parameter	Units	Value	Definition
K_{mf}	mM	0.00008	Forward-mode Ca^{2+} affinity of the SERCA pump
K_{mr}	mM	4.5	Reverse-mode Ca^{2+} affinity of the SERCA pump
τ_{tr}	ms	40	Time constant for Ca^{2+} transport from the network to junctional SR
K_{up}	mM	0.0006	Half-maximal $[Ca^{2+}]_i$ for Ca^{2+} uptake in the NSR
K_{mfCA}	mM	0.00035	Dissociation constant of Ca^{2+}-dependent inactivation of I_{CaL}
α_{fCa}	ms^{-1}	0.021	Ca^{2+} dissociation rate constant for I_{CaL}
Membrane parameters			
g_{sus}	nS/pF	0.0156	Normalized conductance for I_{sus} channels
g_{bNa}	nS/pF	0.0049	Normalized conductance for I_{bNa} channels
g_{K1}	nS/pF	0.0323	Normalized conductance for I_{K1} channels
g_{Ks}	nS/pF	0.012	Normalized conductance for I_{Ks}channels
g_{Na15}	nS/pF	0.000237	Normalized conductance for I_{Na15} channels
g_{Na11}	nS/pF	0.000237	Normalized conductance for I_{Na11} channels
g_{CaL12}	nS/pF	0.2832	Normalized conductance for I_{Na12} channels
g_{CaL13}	nS/pF	0.9936	Normalized conductance for I_{Na13} channels
g_{CaT}	nS/pF	0.5600	Normalized conductance for I_{CaT} channels
g_{If}	nS/pF	0.228	Normalized conductance for I_{If} channels
g_{Kr}	nS/pF	0.0960	Normalized conductance for I_{Kr} channels
g_{to}	nS/pF	0.1968	Normalized conductance for I_{to} channels
K_{NaCa}	pA/pF	220	Scaling factor for I_{NaCa}
g_{bCa}	nS/pF	0.0006	Normalized conductance for I_{bCa} channels
g_{bK}	nS/pF	0.0001	Normalized conductance for I_{bK} channels
I_{NaKmax}	pA/pF	5.698	Maximal Na/K pump current conductance
K_{mNa}	mM	14	Half-maximal $[Na^+]_i$ for I_{NaK}
K_{mK}	mM	1.4	Half-maximal $[K^+]_o$ for I_{NaK}
AC-cAMP/PKA signaling parameters in the numerical model			
$K_{AC,I}$	1/min	0.016	Non-Ca^{2+} AC activity
K_{AC}	1/min	0.0735	Non-Ca^{2+} AC activation
K_{Ca}	mM	0.000178	Maximal Ca^{2+} AC activation
$K_{AC,Ca}$	mM	0.000024	Half-maximal Ca^{2+} AC activation
k_{PKA}	pmol/protein/min	9,000	Maximal PKA activity
$k_{PKA,cAMP}$	pmol/protein	284.5	Half-maximal PKA activation
n_{PKA}		5	Hill coefficient
Phosphorylation parameters			
k_{PLBp}	1/min	52.25	Maximal PLB phosphorylation
n_{PLB}		1	Hill coefficient
$k_{PKA,PLB}$		1.651	Half-maximal PLB phosphorylation
[PP1]	μM	0.89	PP1 concentration
k_{PP1}	1/μM/min	23.575	Maximal PP1 activity
$K_{PP1,PLB}$		0.06967	Half-maximal PP1 activity
Force parameters			
SL_0	μm	0.8	Constant coefficient that describes the effect of actin- and myosin-filament lengths on the single overlap length
N_c	$1/mm^2$	2×10^{13}	SAN cross-section area
F_{k0}	1/mM	350	Cross-bridge–independent coefficient of calcium
F_{k1}	1/mM	3,000	Cooperativity coefficient; describes the dependence of calcium affinity on the number of strong cross-bridges
FN		3.5	Hill coefficient
$F_{k,0.5}$	$1/mm^3$	2.5×10^9	Half-maximal cross-bridge Ca^{2+} affinity
F_{k1}	1/mM/ms	60	Rate constant of calcium binding to troponin
F_f	1/ms	0.04	Cross-bridge turnover rate from the weak to the strong conformation
F_{g0}	1/ms	0.03	Cross-bridge weakening rate under the isometric regimen
F_{gl}	1/m	4.4×10^6	Mechanical-feedback coefficient; describes the dependence of the cross-bridge weakening rate on the shortening velocity
F_{xb}	mN	2×10^{-9}	Unitary force per cross-bridge under the isometric regimen
ATP parameters			
$ATP_{i,max}$	mM	0.02533	
k_{ATP}		61,420	
$k_{ATP,0.5}$		6,724	
cAMPb		20	Baseline cAMP concentration
$K_{ATP,min}$		6,034	
n_{ATP}		3.36	
Caged experiments			

Table S2. **Model constants** *(Continued)*

Model parameter	Units	Value	Definition
$k_{cAMP,on}$	$mM^{-1}\ ms^{-1}$	10^{-5}	Rate of cAMP caging
$k_{cAMP,off}$	ms^{-1}	0.3	Rate of cAMP release from the cage

REFERENCES

Catanzaro, J., M. Nett, M. Rota, and M. Vassalle. 2006. On the mechanisms underlying diastolic voltage oscillations in the sinoatrial node. *J. Electrocardiol.* 39:342. http://dx.doi.org/10.1016/j.jelectrocard.2006.03.006

Demir, S.S., J.W. Clark, and W.R. Giles. 1999. Parasympathetic modulation of sinoatrial node pacemaker activity in rabbit heart: A unifying model. *Am. J. Physiol. Circ. Physiol.* 276:H2221–H2244.

Kharche, S., J. Yu, M. Lei, and H. Zhang. 2011. A mathematical model of action potentials of mouse sinoatrial node cells with molecular bases. *Am. J. Physiol. Circ. Physiol.* 301:H945–H963. http://dx.doi.org/10.1152/ajpheart.00143.2010

Kurata, Y., I. Hisatome, S. Imanishi, and T. Shibamoto. 2002. Dynamical description of sinoatrial node pacemaking: Improved mathematical model for primary pacemaker cell. *Am. J. Physiol. Circ. Physiol.* 283:H2074–H2101. http://dx.doi.org/10.1152/ajpheart.00900.2001

Larson, E.D., J. Clair, W.A. Sumner, J.R. St Clair, W.A. Sumner, R.A. Bannister, and C. Proenza. 2013. Depressed pacemaker activity of sinoatrial node myocytes contributes to the age-dependent decline in maximum heart rate. *Proc.* 110:18011–18016.

Liu, J., S. Sirenko, M. Juhaszova, S.J. Sollott, S. Shukla, Y. Yaniv, and E.G. Lakatta. 2014. Age-associated abnormalities of intrinsic automaticity of sinoatrial nodal cells are linked to deficient cAMP-PKA-Ca2+ signaling. *Am. J. Physiol. Heart Circ. Physiol.* 306:H1385–H1397. http://dx.doi.org/10.1152/ajpheart.00088.2014

Luo, C., and Y. Rudy. 1994. A dynamic model of the cardiac ventricular action potential. I. Simulations of ionic currents and concentration changes. *Circ. Res.* 74:1071–1096. http://dx.doi.org/10.1161/01.RES.74.6.1071

Maltsev, V.A., and E.G. Lakatta. 2010. A novel quantitative explanation for the autonomic modulation of cardiac pacemaker cell automaticity via a dynamic system of sarcolemmal and intracellular proteins. *Am. J. Physiol. Circ. Physiol.* 298:H2010–H2023. http://dx.doi.org/10.1152/ajpheart.00783.2009

Saucerman, J.J., L.L. Brunton, A.P. Michailova, and A.D. McCulloch. 2003. Modeling β-adrenergic control of cardiac myocyte contractility in silico. *J. Biol. Chem.* 278:47997–48003. http://dx.doi.org/10.1074/jbc.M308362200

Yaniv, Y., R. Sivan, and A. Landesberg. 2005. Analysis of hystereses in force length and force calcium relations. *Am. J. Physiol. Circ. Physiol.* 288:H389–H399. http://dx.doi.org/10.1152/ajpheart.00722.2003

Yaniv, Y., A. Ganesan, D. Yang, B.D. Ziman, A.E. Lyashkov, A. Levchenko, J. Zhang, and E.G. Lakatta. 2015. Real-time relationship between PKA biochemical signal network dynamics and increased action potential firing rate in heart pacemaker cells: Kinetics of PKA activation in heart pacemaker cells. *J. Mol. Cell. Cardiol.* 86:168–178.